P-04-283

Forsmark site investigation

Test of the analytical signal technique and Euler deconvolution on Forsmark data

Mehrdad Bastani, Leif Kero
Geological Survey of Sweden

December 2004

Svensk Kärnbränslehantering AB
Swedish Nuclear Fuel
and Waste Management Co
Box 5864
SE-102 40 Stockholm Sweden
Tel 08-459 84 00
+46 8 459 84 00
Fax 08-661 57 19
+46 8 661 57 19

ISSN 1651-4416
SKB P-04-283

Forsmark site investigation

Test of the analytical signal technique and Euler deconvolution on Forsmark data

Mehrdad Bastani, Leif Kero
Geological Survey of Sweden

December 2004

Keywords: Airborne geophysics, Analytic signal technique, Euler deconvolution, AP PF 400-03-99.

Abstract

The analytical signal (AS) and Euler deconvolution (ED) techniques have been used to process airborne magnetic total field data from the Forsmark area. The AS technique makes use of densely sampled data along the flight lines and the ED uses grid data.

In order to show the reliability and correctness of the estimated source parameters (dip, depth, strike and width) both methods were tested on a set of synthetic data. The test showed that the estimates are well reflecting the true source parameters as long as the basic assumptions are met. The ED method proved to be more versatile for the depth estimations. The synthetic data were also used to establish some guidelines to the filtering of the estimates in locations were the basic assumptions concerning the AS technique were violated.

The results from the data processing in the Forsmark area with the AS technique show that the estimated source parameters are stable and can be used to automatically detect the elongated structures. The dips and the strikes estimated by the AS technique and those measured by means of the anisotropy of magnetic susceptibility (AMS) method (laboratory measurements on oriented surface samples) are very well correlated.

The ED method is applicable even if no simple model can properly represent the geological setting. Different structural indices; sphere (3), pipe (2), sill/dyke (1), thick step (0.5) and magnetic contact (0) have been used to estimate the depth to the top of causative bodies in the Forsmark area. Most frequently a magnetic contact model has been utilised. Different search window and grid sizes have been used to include single target anomalies. A few wider windows were also used to study the deeper sources (a few hundred metres).

Sammanfattning

Analytisk signal (AS) och Euler dekonvolution (ED) har använts för att bearbeta flygmätta magnetiska totalfältsdata från Forsmarksområdet. AS-metoden använder sig av tätmätta linjedata och ED använder sig av data i grid.

För att kunna visa tillförlitligheten och precisionen av de beräknade modellparameterna (stupning, djup, strykning och bredd) testades båda metoderna på ett syntetiskt dataset. Testet visade att beräkningarna väl speglar de riktiga modellparametrarna när de för metoden grundläggande antagandena är uppfyllda. Syntetiska data användes även för att ta fram några regler för diskriminering av lösningar där de grundläggande antagandena inte är uppfyllda.

Resultatet från databearbetningarna i Forsmarksområdet med AS-metoden visar att de beräknade modellparametrarna är stabila och kan användas för att automatiskt detektera linjära strukturer. Stupningar och strykningar beräknade med AS-metoden stämmer väl överens med de som erhållits med hjälp av laboratoriemätningar på orienterade ytprov.

ED-metoden förutsätter ej någon speciell geologisk modell och är sålunda användbar även om inte någon speciell modell kan representera geologin. Stukturindex för sfär (3), pipa (2), sill/gång (1), tjockt step (0,5) och magnetisk kontakt (0) har använts vid processeringen, men vanligen index för magnetisk kontakt. Olika storlekar på beräkningsfönstren och gridceller har använts för att optimera anomaliorsaker av olika dimensioner. Några breda fönster har använts för att få strukturell information från djupare liggande orsaker (några hundra meter).

Contents

1 Background and objective

This document reports the interpretation of magnetic data gained from a helicopter borne geophysical survey /Rönning et al. 2003/, which is one of the activities performed within the site investigation at Forsmark. The airborne survey was performed by the Geological Survey of Norway (NGU) along both NS and EW oriented survey lines and with a line spacing of 50 m, see Figure 2-1.

Interpretation of the acquired magnetic total field data has been carried out, applying the analytic signal technique and Euler deconvolution. The interpretation results comprise strike, dip and depth to magnetic anomaly sources.

The activity has been carried out according to the activity plan AP PF 400-03-93 (SKB internal controlling document). The activity plan included Euler deconvolution only, but the work was later extended to also include the analytic signal technique. Rune Johansson (SKB activity leader) assisted in editing the report.

Figure 1-1. *The area covered by geophysical measurements from helicopter. Measurements are performed along north-south lines in the large diamond shaped area and along east-west lines in the smaller area.*

2 Analytic signal technique

/Bastani and Pedersen, 2001/ have shown that the analytic signal of the magnetic field data can be used to automatically determine the source parameters (dip, depth to the top and strike) of dike-like structures. The method is particularly useful for interpreting large amounts of data collected during airborne surveys because it makes full use of the high density of data along the flight lines, while at the same time checking for two-dimensionality and strike directions by searching for coherent signals in neighbouring profiles. The model used is an infinite thin dike with a certain strike and dip. To interpret real geological structures, this model has been extended to accommodate dikes with finite width.

2.1 Theoretical background

2.1.1 General theory

The analytical signal, A(x,z), of the magnetic field is a complex function with a real part (A_r) defined as the original field ΔT, and an imaginary part (A_i) as the Hilbert transform of ΔT /Blakely, 1995/. The analytical signal of the magnetic field measured along profiles crossing an infinitely thin dike contains information about the source parameters. It is shown that, assuming an induced magnetisation, the dip of such a dike is given by

$$\vartheta_d = 2\ \vartheta_f - \vartheta_e$$

where ϑ_f and ϑ_e are the phase factors for field component and the effective dip angle, respectively. ϑ_f is a function of the ambient magnetic field which in the wave number domain has a simple expression

$$\Theta_f = \hat{f}_z + i\,\mathrm{sgn}(k)\,\hat{f}_{x,}$$

where subscripts denote Cartesian components in the plane perpendicular to the strike of the field direction. This plane is described by co-ordinates x and z and the strike direction lies in the y-direction, making an angle D_s with the x-axis of the geomagnetic co-ordinate system which points towards geomagnetic north. ϑ_e, the effective dip angle, is a function of the analytic signal and its horizontal and vertical derivatives as

$$\vartheta_e = -\tan^{-1}\frac{A_i}{A_r} + \tan^{-1}\left(\frac{\dfrac{\partial |A(x,z)|}{\partial z}}{\dfrac{\partial |A(x,z)|}{\partial x}}\right)$$

The profile direction may differ from the x-axis, i.e. the direction perpendicular to the strike. However, the analytic signal calculated along the profile direction, using a Fourier transform technique, will be correctly represented in the space domain. Also the ratio between vertical and horizontal derivative of the analytical signal will correctly describe the angle ϑ_x.

The interpretation of the angle ϑ_e does require some caution. All angles relate to the x-z plane. The true magnetisation and normal field vectors must be projected onto the x-z plane before the dip angle ϑ_d can be found. Projecting the normal field vector onto the x-z plane yields

$$\vartheta_f = \tan^{-1}\left(\frac{\tan I}{\sin(D_s - D)}\right)$$

where D_s is the dyke's strike. I and D are the normal field's inclination and declination, respectively.

2.1.2 Depth and with determination

Structures with finite widths affect the curvature of the analytic signal and its derivatives. Accounting for these effects will improve depth estimations. The depth, d, and the half width, a of such structure is given by

$$d = \frac{-i\,R(0)}{1 + real(S(0))}$$

and

$$a = d\left[\frac{2iR(0)}{d} - 1\right]^{1/2}$$

where

$$R(x) \equiv \frac{A_x^{(1)}}{A_x^{(2)}} = \frac{\dfrac{1}{d - i(x-a)} - \dfrac{1}{d - i(x+a)}}{\dfrac{i}{[d - i(x-a)]^2} - \dfrac{i}{[d - i(x+a)]^2}}$$

and

$$S(x) = \frac{\partial R}{\partial x} = \frac{1}{2i}\frac{p^*(-2i)p - i(p^2 + a^2)}{(p^*)^2}$$

with $p = d - ix$. $A_x^{(1)}$ and $A_x^{(2)}$ are the 1st and the 2nd horizontal derivatives of the analytic signal, respectively.

2.1.3 Strike determination

In order to project the normal magnetic field vector onto the x-z plane, the strike of the dike must be known. It is assumed that many short wavelength magnetic anomalies are caused by linear dyke-like structures. At the first stage the dikes are located by using the second horizontal derivative of analytic signal. Then, by considering the profile separation and sampling distance along the profiles, a search radius and a stacking window with length equal to J data points is defined. In the next stage, a model trace is defined as the measured anomaly over the stacking window minus the mean value over that interval. The mean removed magnetic anomalies over the same length for a certain number of neighbouring

traces (I-1) is then estimated by shifting the model trace along slanting lines of varying strikes, α. For each α the prediction error energy over the length J and the number of neighbouring lines (I-1) is computed according to

$$E(\alpha)= \frac{1}{(I-1)J}\sum_{i=1}^{I}\sum_{j=1}^{J}[d_j - \hat{d}_{ij}(\alpha)]^2$$

The estimated strike is the angle that minimises the prediction error E

Strike = $\alpha_{E\min}$

2.1.4 Identifying contacts and dikes

/Blakely, 1995/ has shown that the horizontal derivative of the magnetic field along a profile over a magnetic contact resembles a signal from an infinitely thin magnetic dike. This concept can be used to estimate the dip and strike of the magnetic contacts. On the other hand, the horizontal derivative operator acts as a high pass filter and if the original signal contains high frequency noise it is highly amplified.

The estimated depth and width can also be used to distinguish dykes and contacts. The estimated width/depth ratio helps to identify the contacts. The contacts are likely represented by large ratios.

2.2 Data processing

Preliminary processing of the Forsmark grid data showed that the method is applicable to the existing data set. The following is a brief description of the processing carried out.

2.2.1 Pre-processing

The program performs automatic strike estimation. If there are some crossing lines in the dataset the program can't find the strikes at the crossing points and it fails. Therefore the data locations were mostly shifted a few meters to avoid crossing lines (Figure 2-1).

The data seemed to be contaminated with high frequency noise (HFN). The noise affects the calculations considerably and distorts the first and the second horizontal derivatives of the analytic signal which are used to calculate the depth to the top of the dikes.

A low-pass filter with a width of 60 m was used to remove the HFN and the data were sampled every 10 m. Figure 2-2 depicts the original data (blue) and the low-pass filtered data along an EW profile.

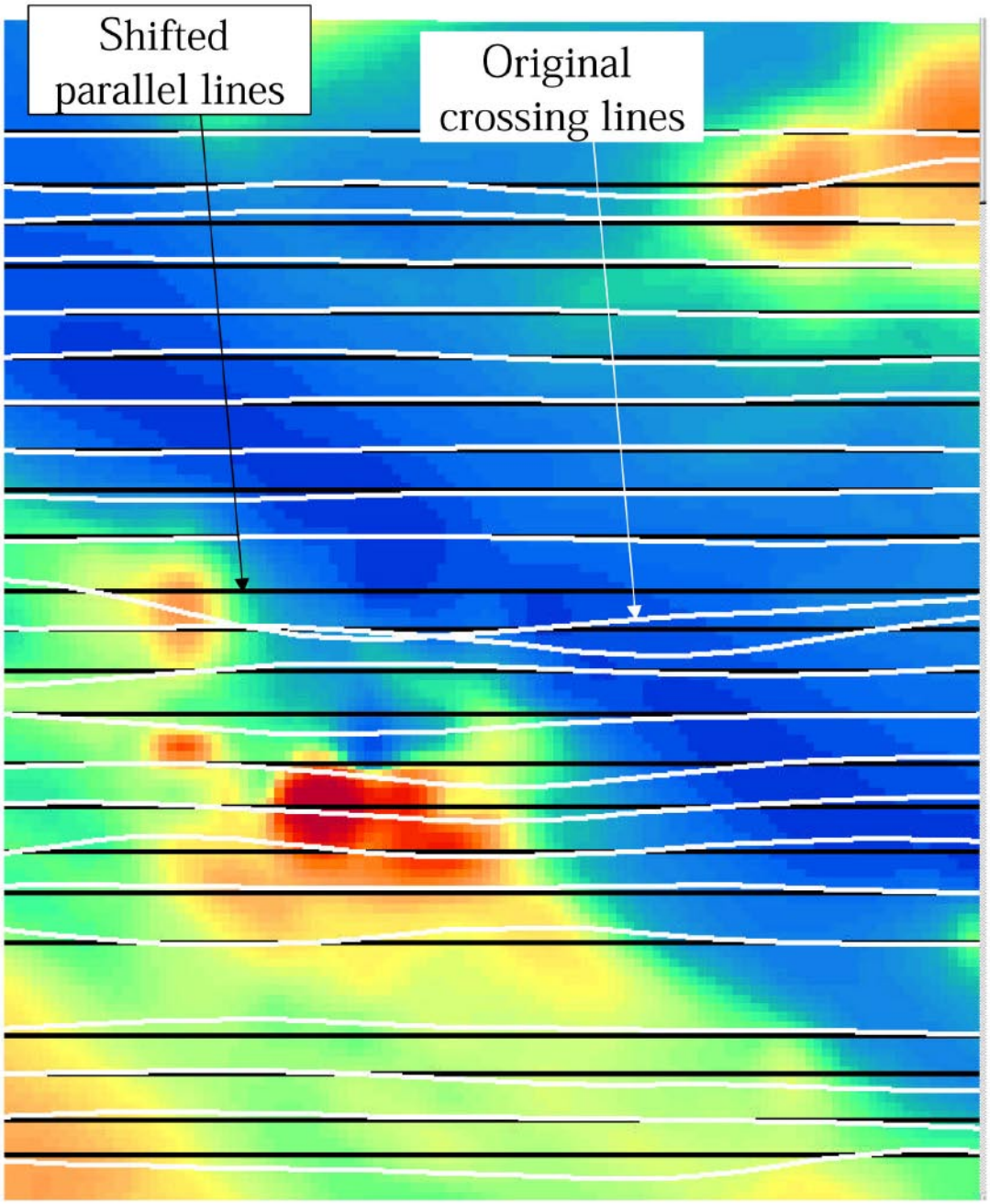

Figure 2-1. *Location of original crossing WE profiles (white) and shifted parallel profiles (black) superimposed on the coloured map of total magnetic field.*

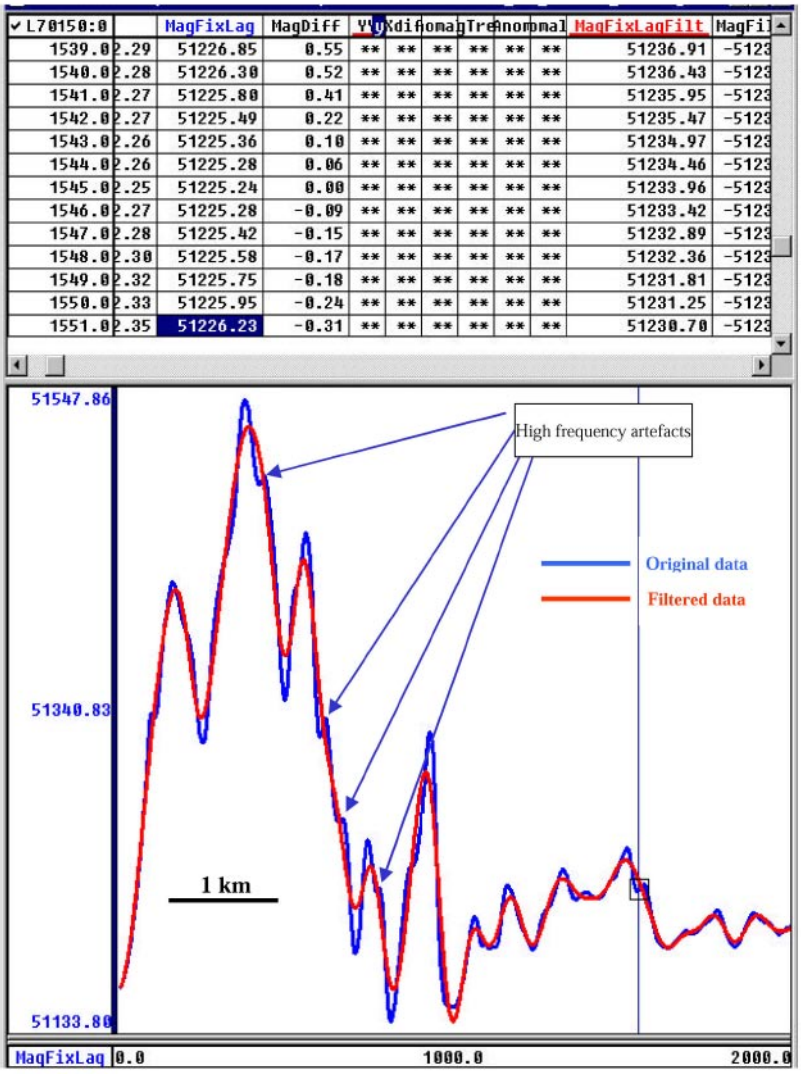

Figure 2-2. *Example of original data (blue plot) contaminated with high frequency noise (marked with arrows). The data is low-pass filtered (red plot) to reduce the noise.*

2.2.2 Processing results

The main processing program, developed at SGU and Uppsala University, is written in MATLAB. All the modules are interfaced to the Geosoft Oasis montaj™ software using GX (Geosoft executables) scripts. The final results are stored in an Oasis montaj database. The database contains the estimated dip, depth, width, and strike of the dyke-like magnetic anomalies. The results can then easily be exported in any desirable format.

For a documentation of the data files produced and delivered to SKB, see section 6.1.

Dip and strike estimations

The dips and strikes were estimated separately for EW and NS data. The models used are a thin dike with positive and negative magnetic signature, respectively. The magnetic anomalies with positive and negative signature as well as the horizontal derivative of the magnetic anomalies with positive signature are used in the processing. The number at each point shows the estimated dip and the symbol indicates the strike (using right-hand rule).

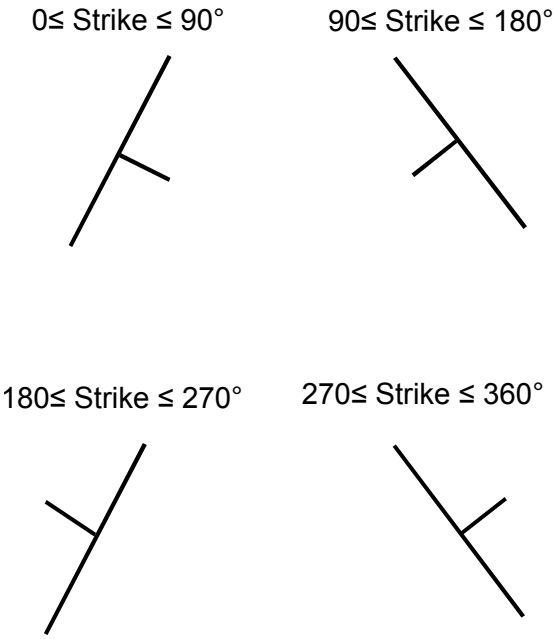

Figure 2-3. *Four possible combinations of dip and strike visualising. The strike and dip vary between 0 to 360° and 0 to 90°, respectively.*

The estimated dips and strikes are usually superimposed on the total magnetic field maps. The right hand rule concept is used to draw the symbols. According to this rule, the right hand is always in the dip direction when standing in the strike direction. Figure 2-3 shows four possible combinations of dip and strike.

Examples of estimated dips and strikes are shown in Figure 2-4 and 2-5.

Depth and width estimations

The estimated depths to the dyke-like magnetic bodies are shown in Figures 2-6 and 2-7. Estimates are shown for positive anomalies (EW and NS data) and negative anomalies (EW and NS data), respectively.

As mentioned in the introduction, the source parameters of a magnetic contact can be estimated in two different ways. The horizontal derivative is the first choice. High frequency noise, however, considerably affects the horizontal derivatives and therefore, the use of the width to depth ratio has been preferred.

In order to compare the results, the estimated depths and ratios for both data sets (EW and NS) were combined and shown in a single map. Figure 2-8 to 2-9 depicts maps of the combined results, namely the estimated depths and width-depth ratios for magnetic anomalies with positive and negative signatures.

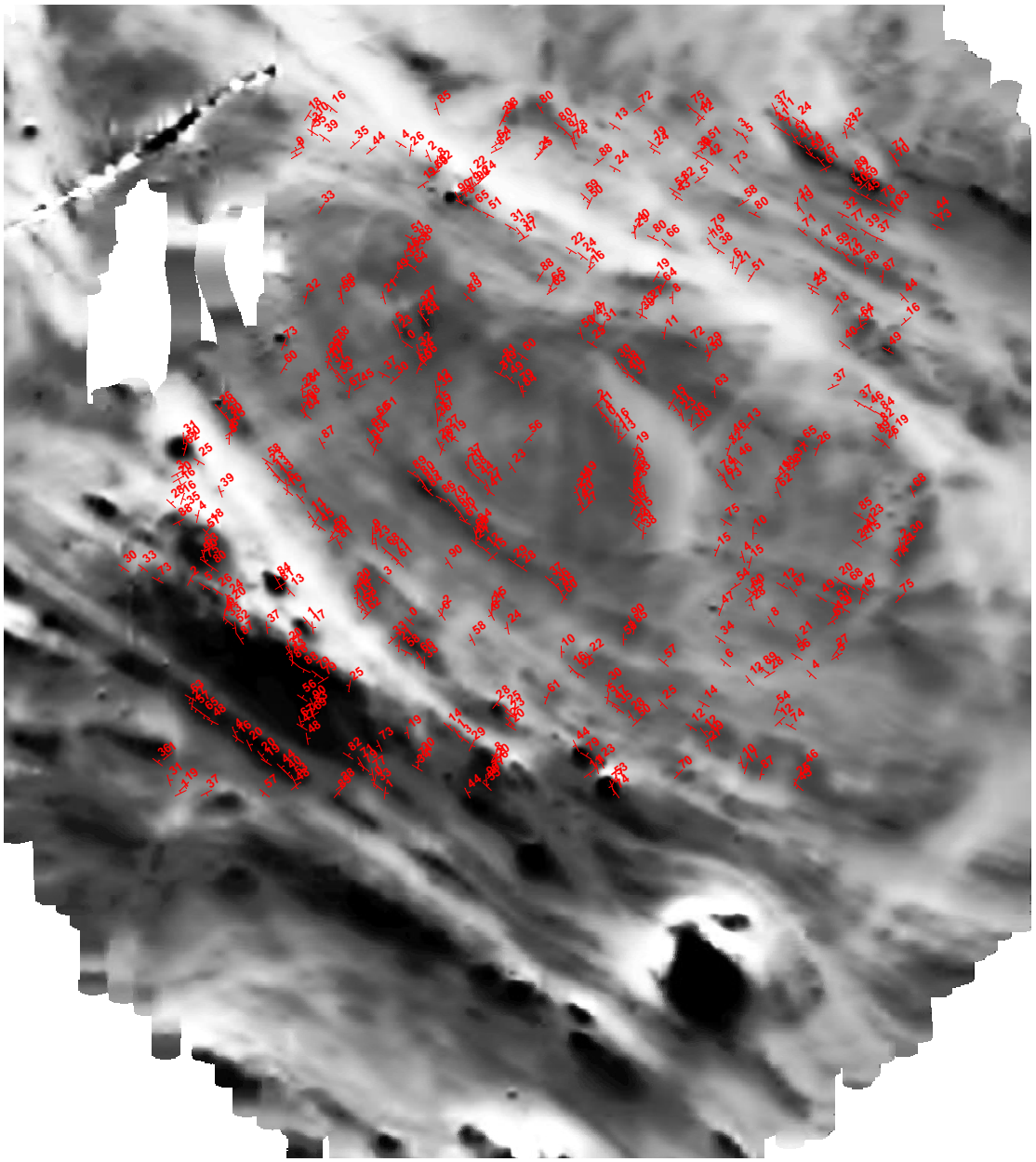

Figure 2-4. *Estimated dips and strikes using the NS data and magnetic anomalies with positive signature. The number at each location is the estimated dip in degrees. The background shows the grey-scaled map of the total magnetic field. Dark and light grey correspond to magnetic highs and lows, respectively. Note that the estimates are limited to certain areas.*

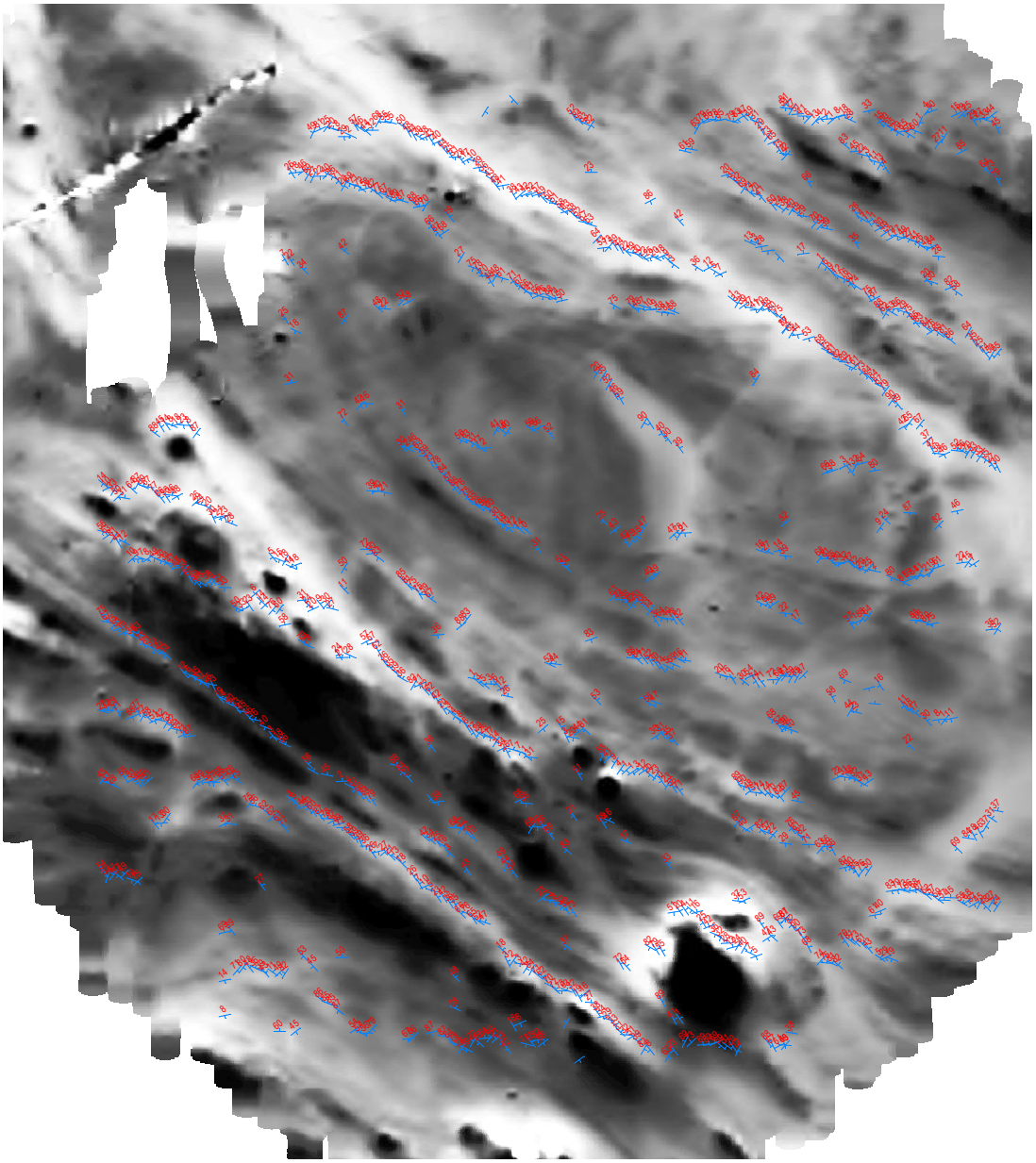

Figure 2-5. *Estimated dips and strikes using the NS data and magnetic anomalies with negative signature. The number at each location is the estimated dip in degrees. The background shows the grey-scaled map of the total magnetic field. Dark and light grey correspond to magnetic highs and lows, respectively. Note that the estimates are limited to certain areas.*

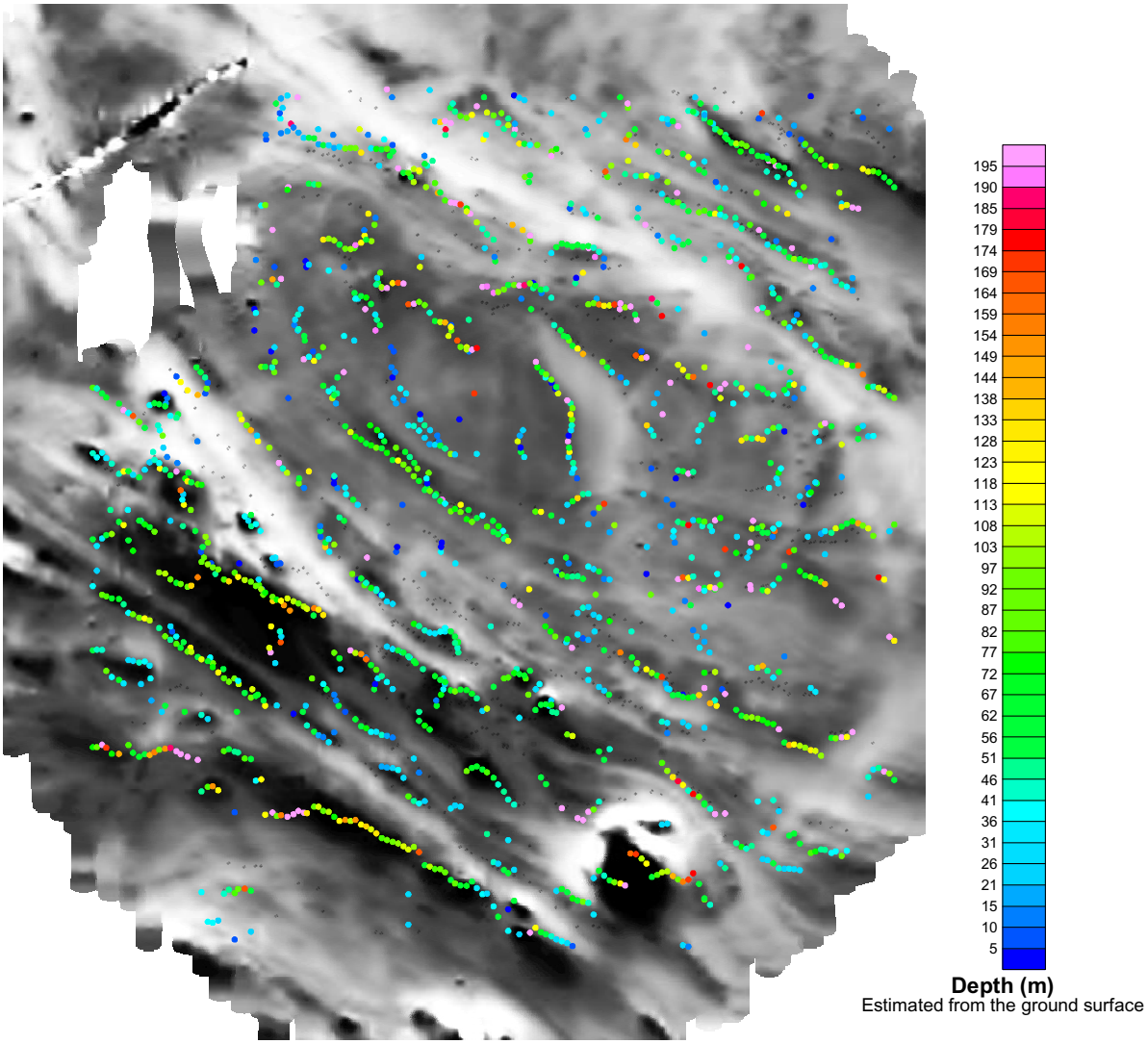

Figure 2-6. *Map of the combined estimates (using NS and EW data). The map shows the depth to the top of causative bodies for the magnetic anomalies with a positive signature. The grey-scaled background shows the total magnetic field. Dark and light grey correspond to magnetic highs and lows, respectively.*

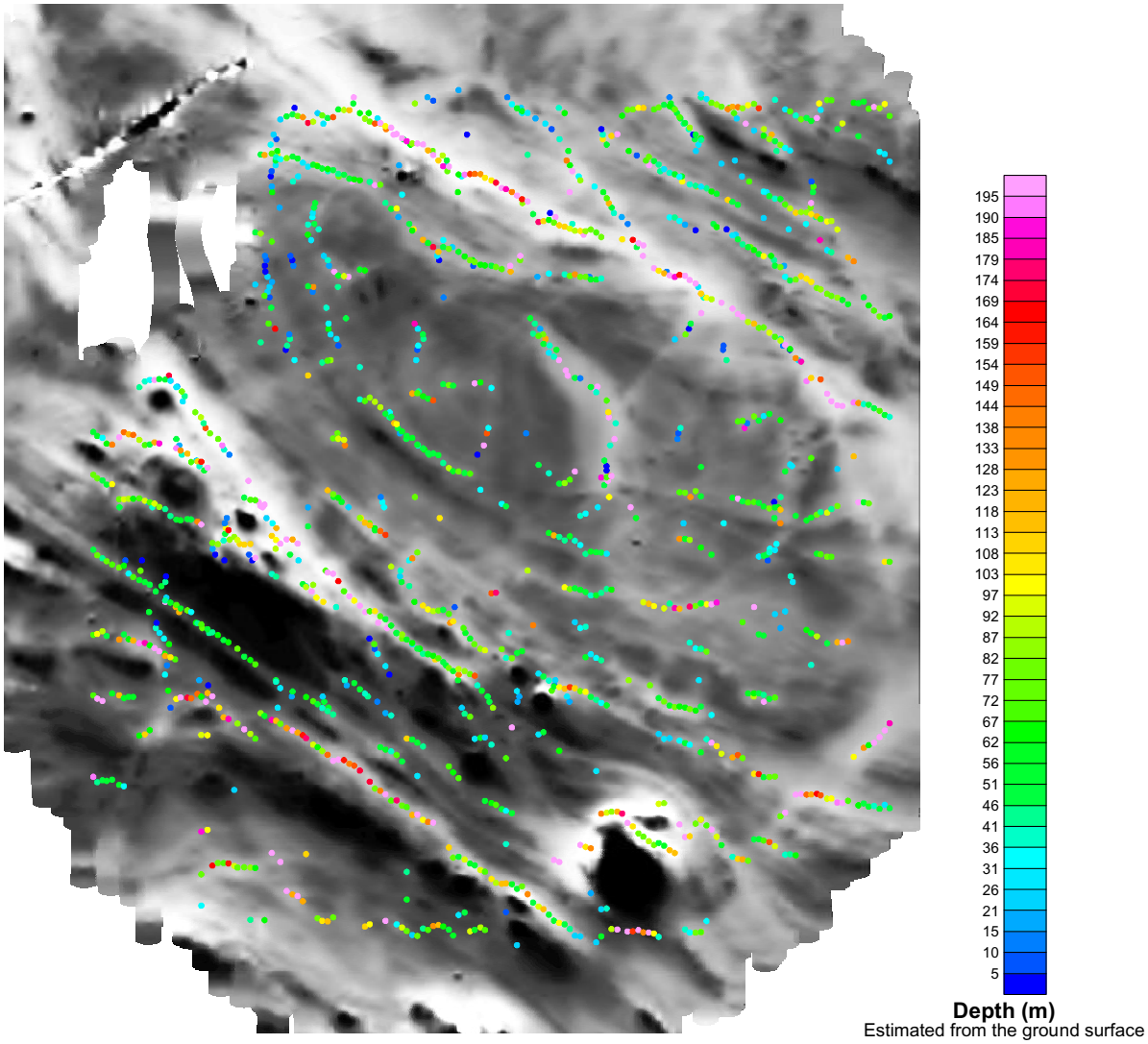

Figure 2-7. *Map of the combined estimates (using NS and EW data). The map shows the depth to the top of causative bodies for the magnetic anomalies with a negative signature. The grey-scaled background shows the total magnetic field. Dark and light grey correspond to magnetic highs and lows, respectively.*

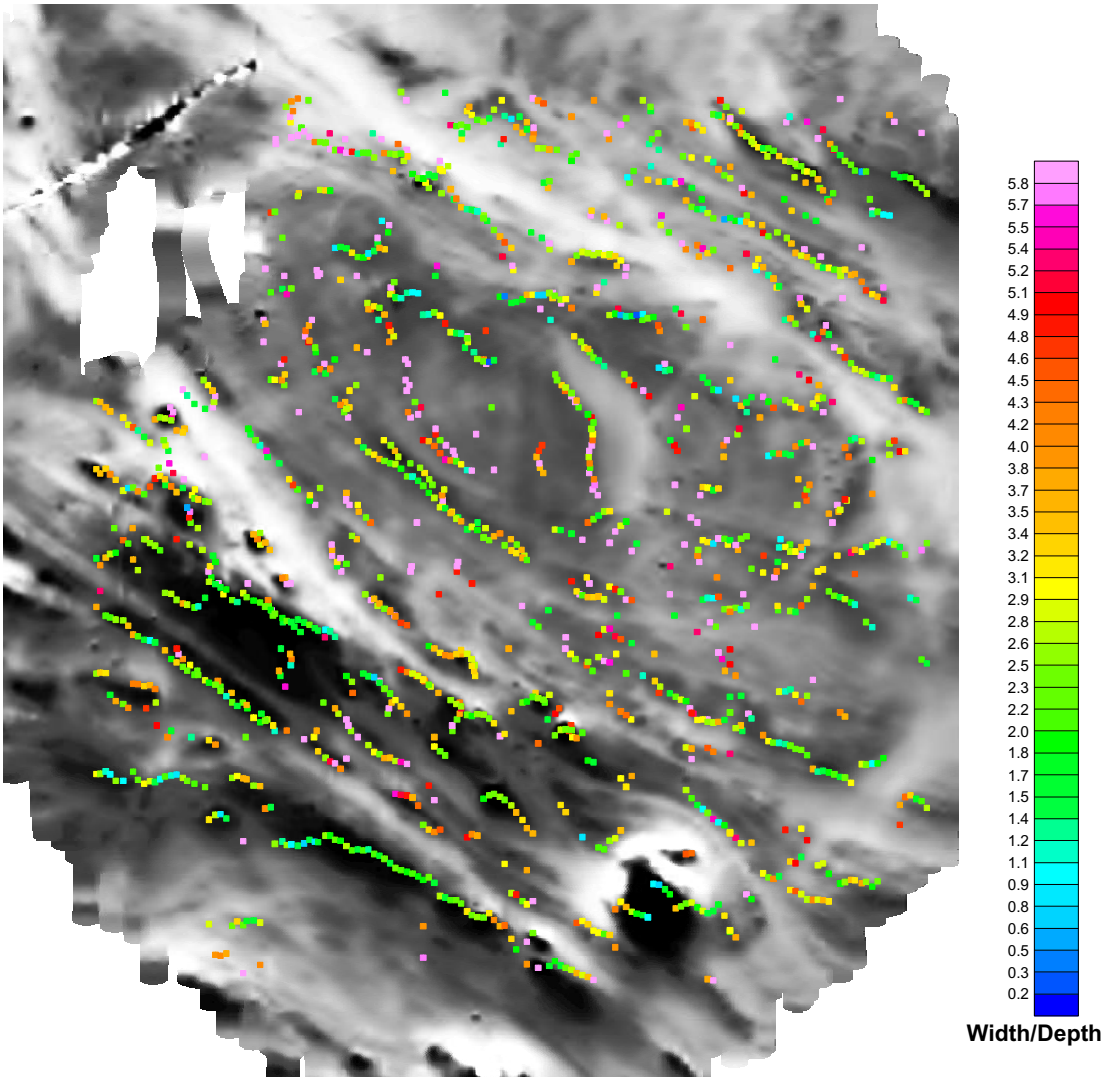

Figure 2-8. *Map of the combined estimates (using NS and EW data). The map shows the width-depth ratio of the causative bodies for the anomalies with a positive signature. The grey-scaled background shows the total magnetic field. Dark and light grey correspond to magnetic highs and lows, respectively.*

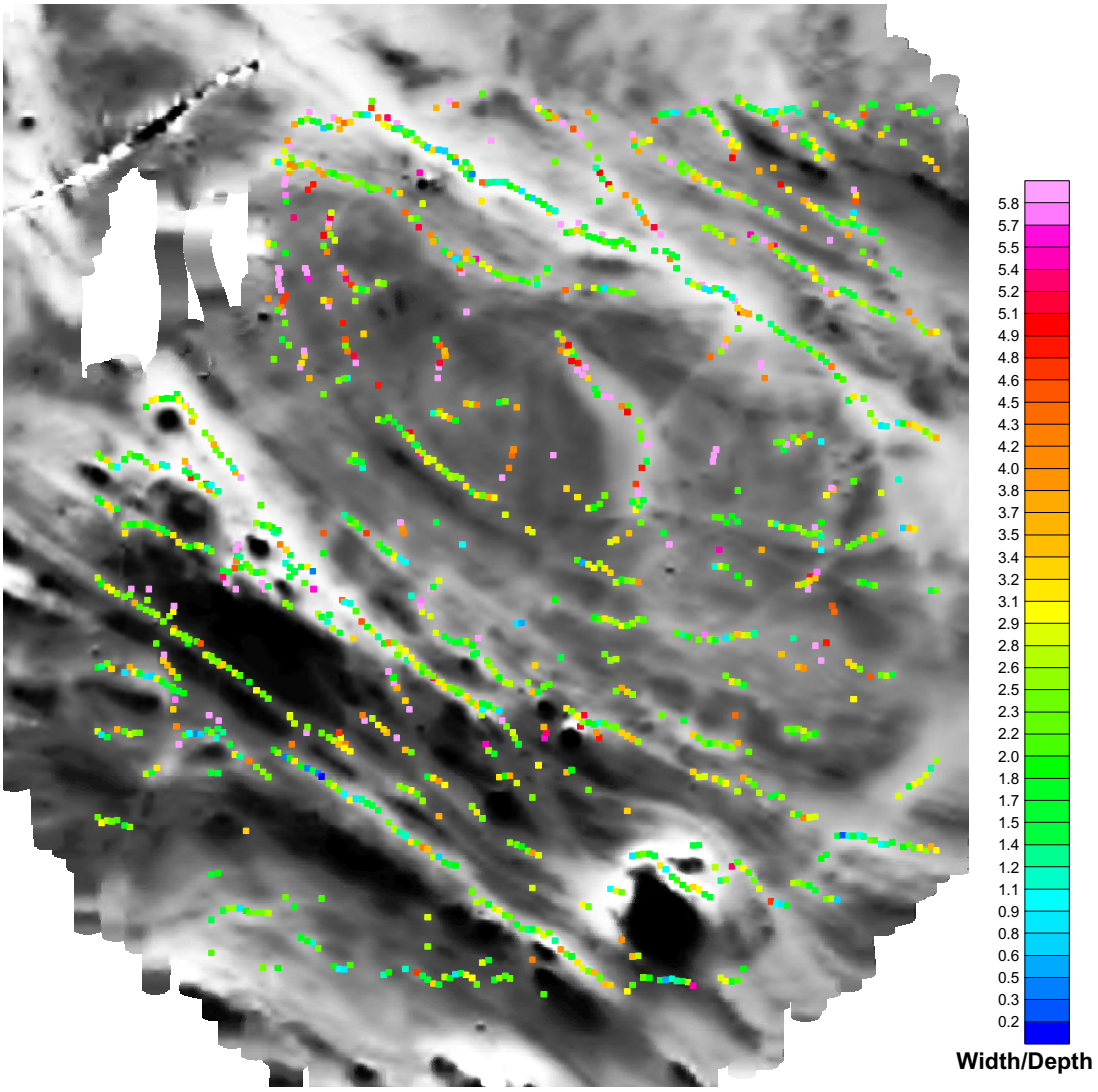

Figure 2-9. *Map of the combined estimates (using NS and EW data). The map shows the width-depth ratio of the causative bodies for the anomalies with a negative signature. The grey-scaled background shows the total magnetic field. Dark and light grey correspond to magnetic highs and lows, respectively.*

3 Euler deconvolution

Leonhard Euler (1707–1783) was a Swiss mathematician who did most of his work in St Petersburg. Together with Lagrange he developed the modern mathematics. He also presented papers in mechanics, physics, astronomy, optics, music and navigation.

PC hardware and software development in recent years and the implementation of the Fast Fourier Transform (FFT) has made it possible to use some of Euler´s theoretical work to evaluate potential field data in practice.

/Thompson, 1982/ has implemented Euler´s theory for 2D, and Reid et al. (1990) for 3D. Euler 3D Deconvolution makes rapid depth estimations from magnetic and gravity data in grid form using Euler´s homogeneity relation. Euler deconvolution is insensitive to magnetic inclination, declination and remanent magnetisation and is very suitable for 3D analyses.

3.1 Theoretical background

Euler's homogeneity relationship for magnetic data can be written in the form:

$$(x - x_0)\frac{\delta T}{\delta x} + (y - y_0)\frac{\delta T}{\delta y}(z - z_0)\frac{\delta T}{\delta z} = N(B - T)$$

where

(x_0, y_0, z_0) is the position of the magnetic source whose total field (T) is detected at (x, y, z,).

B is the regional magnetic field.

N is the measure of the fall-off rate of the magnetic field and may be interpreted as the structural index (SI).

The structural index (SI) defines the type of target used in the Euler deconvolution procedure. Structural indexes can be used for many various geological situations. A sill edge, dike, or fault with a limited throw is best displayed with an index of 1.0, while a fault with large throw is best displayed with a zero index /Reid et al. 1990/. Although the structural index approach to source description does not include irregular boundaries, irregular sill-like bodies can be well delineated by the Euler method with an index of 1.0, while irregular contacts are well shown with a zero index /Reid et al. 1990/.

Table 3-1 displays some examples of magnetic targets relevant to geological interpretation and their corresponding structural indices.

Table 3-1. Magnetic targets and the corresponding structural indices.

Magnetic target	Structural index (SI)
Sphere	3
Cylinder	2
Pipe	2
Sheet	1
Sill	1
Step	0.5
Contact	0

3.2 Data processing

3.2.1 Pre-processing

The two magnetic grids provided by SKB (data from NS and EW flights, both with 10 m grid cell size) were reduced to the pole using the local values for the magnetic inclination I = 73º and the magnetic declination I = +3º. All processing was made with the program Oasis montaj™ from Geosoft Inc. The grids were then re-gridded to a grid cell size of 25 m and 100 m, respectively, and the latter was upward continued to 500 m and 1,000 m in the pre-processing stage. The ground clearance data were gridded separately for the NS flight lines and the EW flight lines.

3.2.2 Processing results

Euler deconvolution was executed within the Geosoft Oasis montaj™ environment employing the program module Euler 3D Deconvolution. The results from the processing are stored in ASCII-files (Geosoft XYZ-files) following the Oasis montaj™ terminology and column names. Some new columns were added to extract a more refined data set of the numerous Euler solutions. The results are furthermore presented in the form of ArcView-tif files. For a documentation of the data files produced and delivered to SKB, see section 6.2.

The processing involves the setting of an appropriate structural index (SI) and using least-squares inversion to solve Euler's homogeneity equation for an optimum of x_o, y_o, z_o and B. A square window size must be specified which is equal to the number of cells in the gridded dataset to be used in the inversion. The window is centred on each of the target locations. All points in the window are used to solve Euler's equation for target depth, inversely weighted by distance from the centre of the window. The window should be large enough to include each target anomaly of interest in the total field magnetic grid, but ideally not large enough to include any adjacent anomalies.

The different window sizes chosen are selected to provide information on the depth to a magnetic contact, dyke, pipe and sphere. A magnetic contact (SI = 0) is the main magnetic structure chosen for this work. The window size is 3×3, 10×10 and 20×20 grid cells and the grid cell size is 10 m, 25 and 100 m.

The calculation height for the 10 m, 25 m, and 100 m grid data was 40 m, 55 m and 130 respectively. The data were upward continued to a height equal to the grid cell size. The coarsely gridded data (100 m grid cell size) were also upward continued to 500 m and 1,000 m.

To be able to refer the depth solutions to the sea level, the airborne radar heights showing ground clearance were combined with a terrain model (10×10 m grid) provided by SKB.

The ED technique produces a considerable number of solutions for a given window size. These solutions must be discriminated in some way. The main discriminating factor chosen was to allow only those solutions that fall within 3 grid cell sizes from the centre of the calculating window. The depth uncertainty was equal to 15%. A few shallow solutions fell above the surface when the ground clearance variations along the lines were corrected for. These are the solutions representing the outcrops. Euler solutions more than 30 m above the sea level (topographic peak value in the area) were rejected.

Figure 3-1 shows the Euler solutions obtained when a 3×3 window and a structural index of 0 (magnetic contact) were used to process the 10 m NS grid-data. Figure 3-2 shows the corresponding solutions based on a 25 m NS grid data using the same processing parameters.

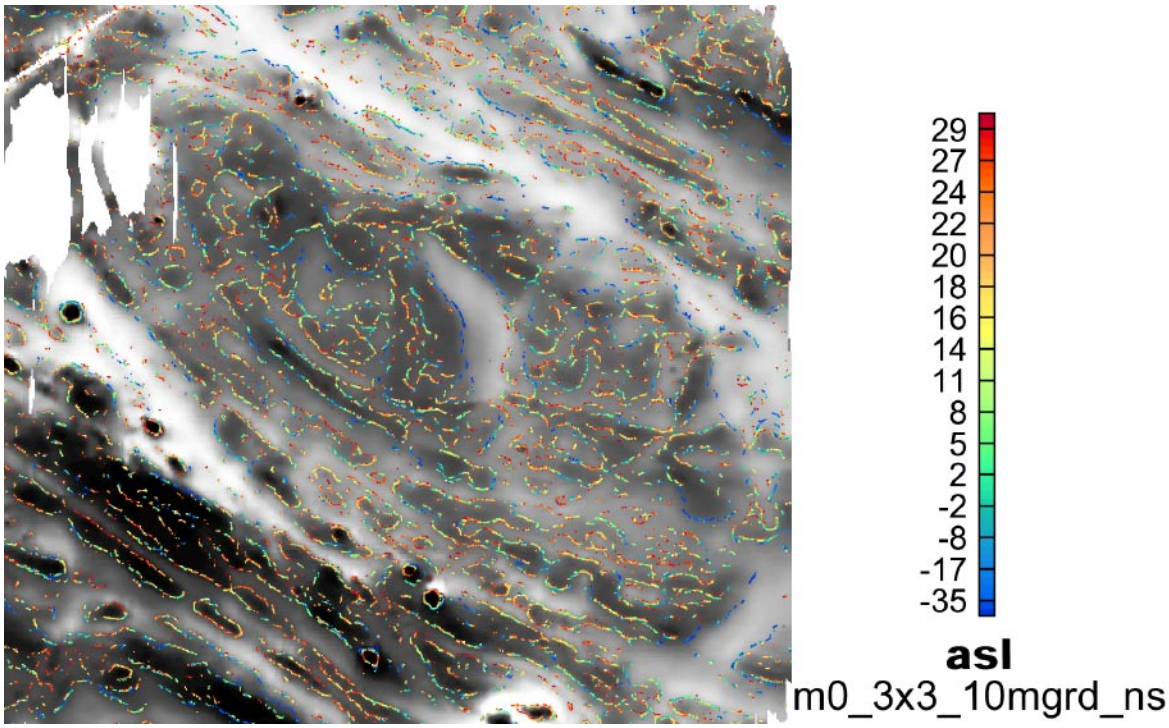

Figure 3-1. *Euler solutions (NS survey, 10 m grid, 3×3 grid cells window, structural index = 0). The background shows the grey-scaled map of the total magnetic field. Dark and light grey correspond to magnetic highs and lows, respectively.*

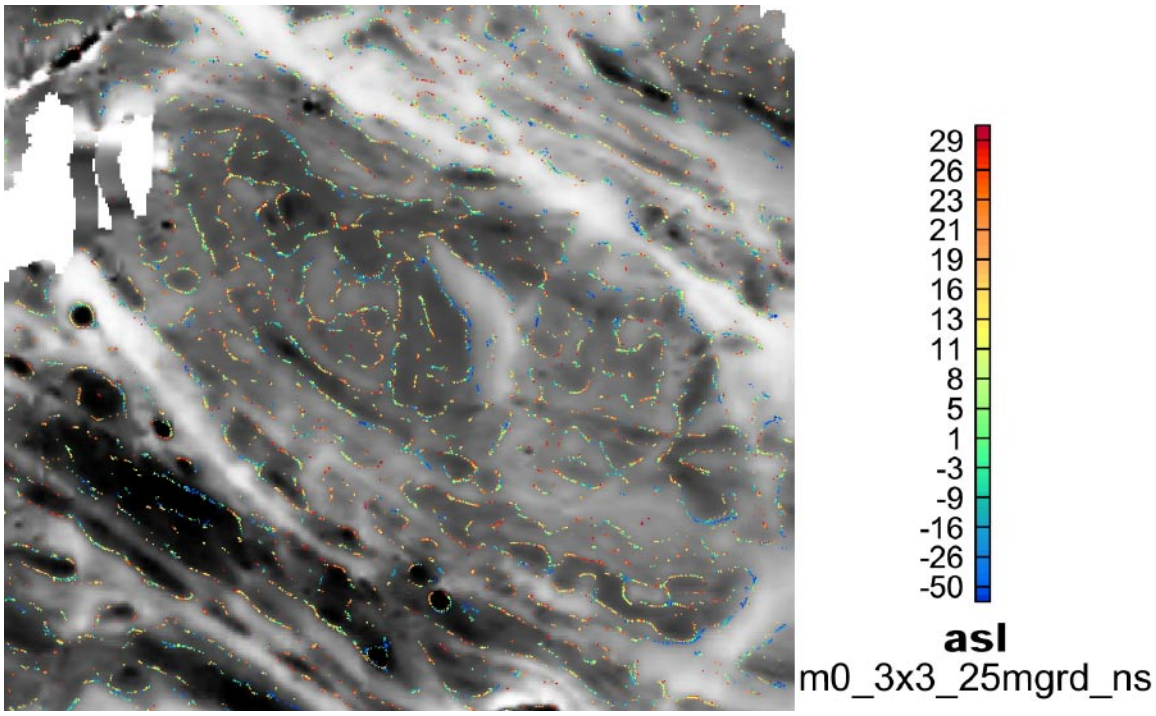

Figure 3-2. *Euler solutions (NS survey, 25 m grid, 3×3 grid cells window, structural index = 0). The background shows the grey-scaled map of the total magnetic field. Dark and light grey correspond to magnetic highs and lows, respectively.*

4 Evaluation of processing results

4.1 Analytic signal technique

The analytical signal technique uses a model which is a thin two-dimensional structure with an infinite length in the direction perpendicular to the measuring profile and an infinite depth extent. In reality, the source parameters are rather more complicated and differ from the simple model used and deviations from these assumptions affect the estimated source parameters considerably. The main sources of error are:

- The limited length of the anomalies perpendicular to the measuring profile.
- The extended width of the anomalies in the profile direction.
- The limited height of the dike (distance from the top to the bottom).
- Presence of parallel and crossing anomalies.
- Strong remanent magnetisation in a direction other than the main magnetic field.
- The edge effect at the starting and ending points.

4.1.1 Synthetic modelling

/Bastani et al. 2002/ have studied the resolution and limitations of the analytical signal method (ASM). The synthetic model displays a few cases where the estimates are biased due to a different true geometry than was used in the ASM processing. The source parameters of five synthetic magnetic bodies are given in Table 4-1. Note that the given strikes and dips are based on the right-hand rule described earlier. Figure 4-1 shows the map of modelled total magnetic field anomaly.

Table 4-1. Source parameters of the causative magnetic bodies used in the synthetic modelling. Width, length and height represent the three dimensions of the body.

No	Width (m)	Length (m)	Height (m)	Strike (deg)	Dip (deg)	Depth (m)
1	200	5,500	4,000	45	90	90
2	200	3,900	4,000	50	65	150
3	400	11,600	4,000	130	70	200
4	400	11,600	4,000	310	70	200
5	50	2,200	400	200	75	20

The synthetic data were processed with ASM and Table 4-2 shows the estimated source parameters at the centre of each body. The strikes are almost perfectly determined and this is very important because errors in strike are directly mapped into the dip estimation. The dip of bodies 1 and 2 are very accurately determined (± 1 degree). For bodies 3, 4 and 5 the dip is overestimated and this might be due to the fact that body 3 and 4 are more than twice as wide as body 1 and 2, and that body 5 has a very limited vertical extension compared to the other bodies. The estimated depths are all overestimated due to deviations from the infinite thin model. In average, the estimated and real depths differ about 10%. The width of structures is resolved poorer compared to the other source parameter with an average relative error of 18%.

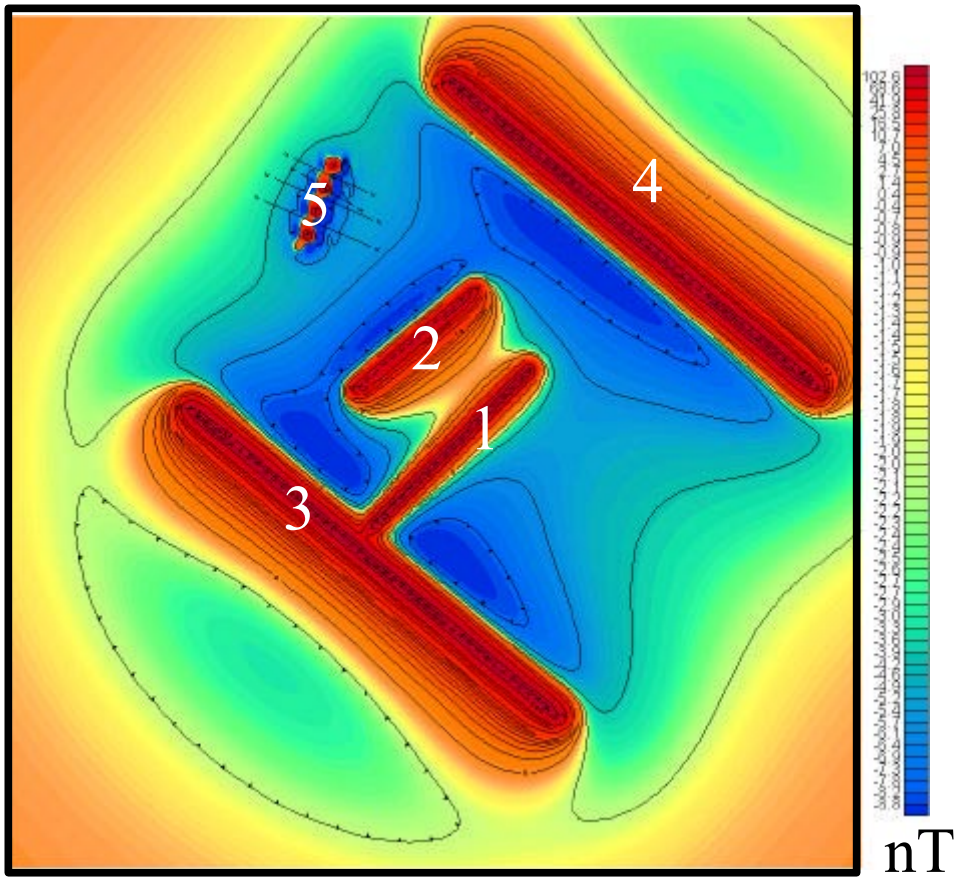

Figure 4-1. *The total magnetic field anomaly and location of causative bodies.*

Table 4-2. The ASM estimated source parameters of the five bodies used in the synthetic moddeling. The two last columns show the ratio between the estimated and true parameters.

No	Strike (deg)	Dip (deg)	Depth (m)	Width (m)	Est. Depth/ True Depth	Est. Width/ True Width
1	45	89	94	250	1,04	1,25
2	51	66	153	227	1,09	1,14
3	129	85	230	320	1,15	0,8
4	311	85	230	320	1,15	0,8
5	204	85	21	60	1,05	1,20

The error sources mentioned above can be analysed by using the results of synthetic modelling.

Length effect

If the anomaly is not extended at least between two lines around the point of estimation, the estimated dip and strike is sometimes considerably biased, see Figure 4-2. This is a hint to reject the estimates when the anomalies have a limited extension. This effect is similar to the edge effect below.

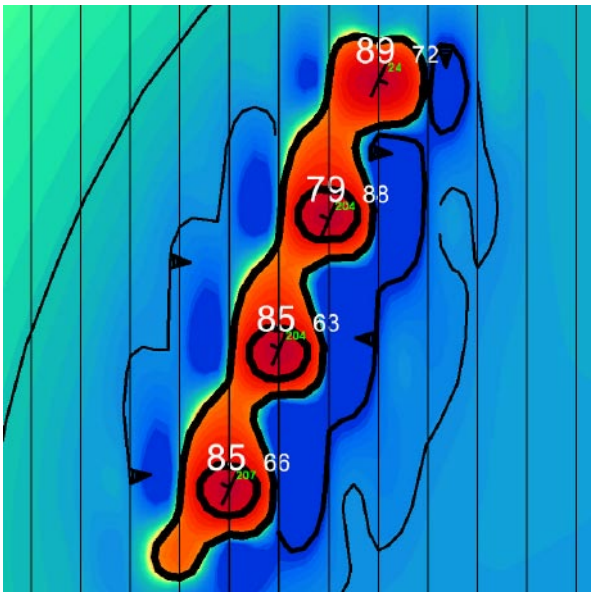

Figure 4-2. *A synthetic example showing the biased dip direction at the northern ending point of body number 5. The dip is shown by large white numbers and the width by smaller white numbers.*

Width effect

Table 4-1 and 4-2 show the bias introduced by increasing width of the anomaly. The dip and depth both become overestimated by increasing the width.

Height effect

The limited height (top to bottom) of the body causes an overestimation of the dip and depth. However it is difficult to separate the height effects from the width effects.

Presence of neighbouring parallel anomalies

In the synthetic model used, the parallel bodies number 1 and 2 were rather far from each other and the estimated source parameters seem to be stable and not affected by the neighbouring anomalies (see Figure 4-3).

Presence of neighbouring crossing anomalies

Synthetic body number 1, at its ending, crosses body number 3 at its middle point. Figure 4-4 shows the zoomed map at the crossing point. The estimated source parameters for body 1 become biased close to the crossing point (estimates inside the white ellipse in Figure 4-4). The dip decreases systematically from 90 (true value) to 45 degrees. The estimated strike increases from 45° to 90° and the depth has an increase of about 30 m. For body number 2, the estimated dip changes direction (points inside the black ellipse in Figure 4-4) with a minimum of 76°. The estimated depth is biased to higher values in the area northwest of the crossing point. The overall conclusion is that the estimated source parameters can be extremely biased at points close to crossing anomalies.

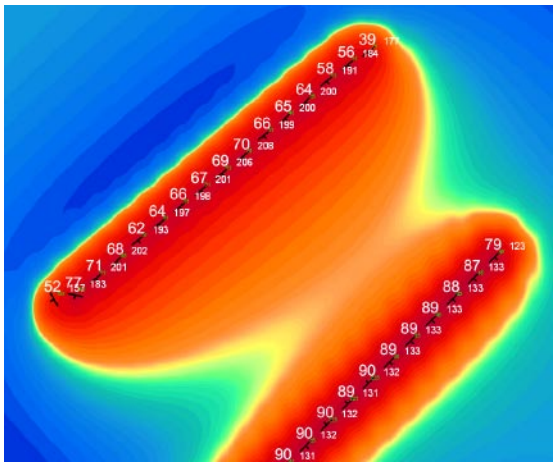

Figure 4-3. *Magnetic anomalies over two parallel dyke-like structures (bodies number 1 and 2 in Figure 4-1). The dip is shown by large white numbers and the width by smaller white numbers.*

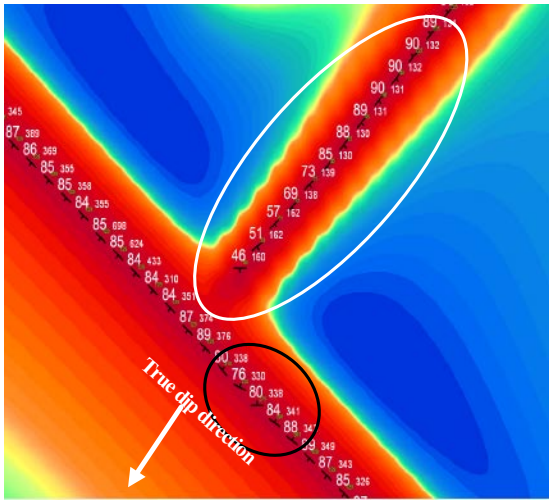

Figure 4-4. *Estimated source parameters superimposed on the map of synthetic magnetic anomalies at the crossing point of bodies 1 and 3 (see Figure 4-1). The dip is shown by large white numbers and the width by smaller white numbers. See text for explanation*

Strong remanent magnetisation

The effect of remanent magnetisation has not been studied by /Bastani et al. 2002/ but the theoretical discussions can be found in /Bastani and Pedersen, 2001/.

The edge effects

The bias at the ending points is mostly due to the deviation from the 2D assumption and lack of correlation between the adjacent profiles. Figure 4-5 illustrates two examples in which the estimated source parameters are highly biased at the ending points of bodies 4 and 5. Note that the bias differs between the two anomalies. Since the magnetic anomaly from body number 5 is more local, the bias is also more local compared to the one from body number 4 (see areas marked by black ellipses).

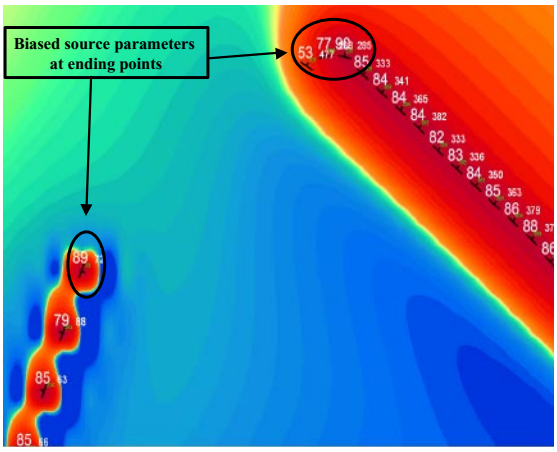

Figure 4-5. *Edge effect on the source parameters. Note that the wider anomaly is more affected by the edge effect. The dip is shown by large white numbers and the width by smaller white numbers. See text for explanation.*

Noise

Noise is an important factor missing in the synthetic modelling presented. All measured data includes random and/or systematic noise which, if not filtered out, may heavily bias the results.

4.1.2 Interpretation of measured data

The synthetic modelling yielded a set of rules and tools to be used when interpreting real data.

- The dip and strike estimates have to be evaluated and interpreted.
- Outliers are filtered out at the ending points of the anomalies.
- The source parameters are rejected for very short anomalies.
- The single point estimations are all filtered out because they show the points where the 2D assumption is extremely violated.
- The outliers at the crossing anomalies are rejected.
- If the estimates along a 2D elongated anomaly show some local scatter the biased estimates are filtered out at that location.
- Wherever the estimated dips have a large scatter the entire set is rejected.
- At points where the anomaly changes the strike abruptly, the effect is similar to the one from crossing anomalies and therefore the results should mostly be rejected.

4.1.3 Interpretation of the Forsmark airborne magnetic data

The estimated source parameters from the EW and NS data have been complied in a single database for the interpretation. Obviously erroneous results have been rejected. For information on the delivered files, XYZ and ArcView tiff files containing refined source parameters, is referred to section 6.1.

The estimates have been superimposed on the map of the total magnetic field to ease the pattern recognition and filtering. Figure 4-6 demonstrates an example containing a complete illustration of the rejection procedure based on the items described in the previous section. The anomaly pattern demonstrates a complicated 3D situation and the solutions belonging to 2D-like features in the anomaly pattern have been selected. The scattered estimations and the local-scatter rejections are most probably due to noise (instrumental and/or geological).

There are some locations in which the scattered dips are nearly vertical and such solutions have been maintained. Figure 4-7 depicts an example of this type. The dip values vary between 79°–89° SSW to 76°–82° NNW (worst case).

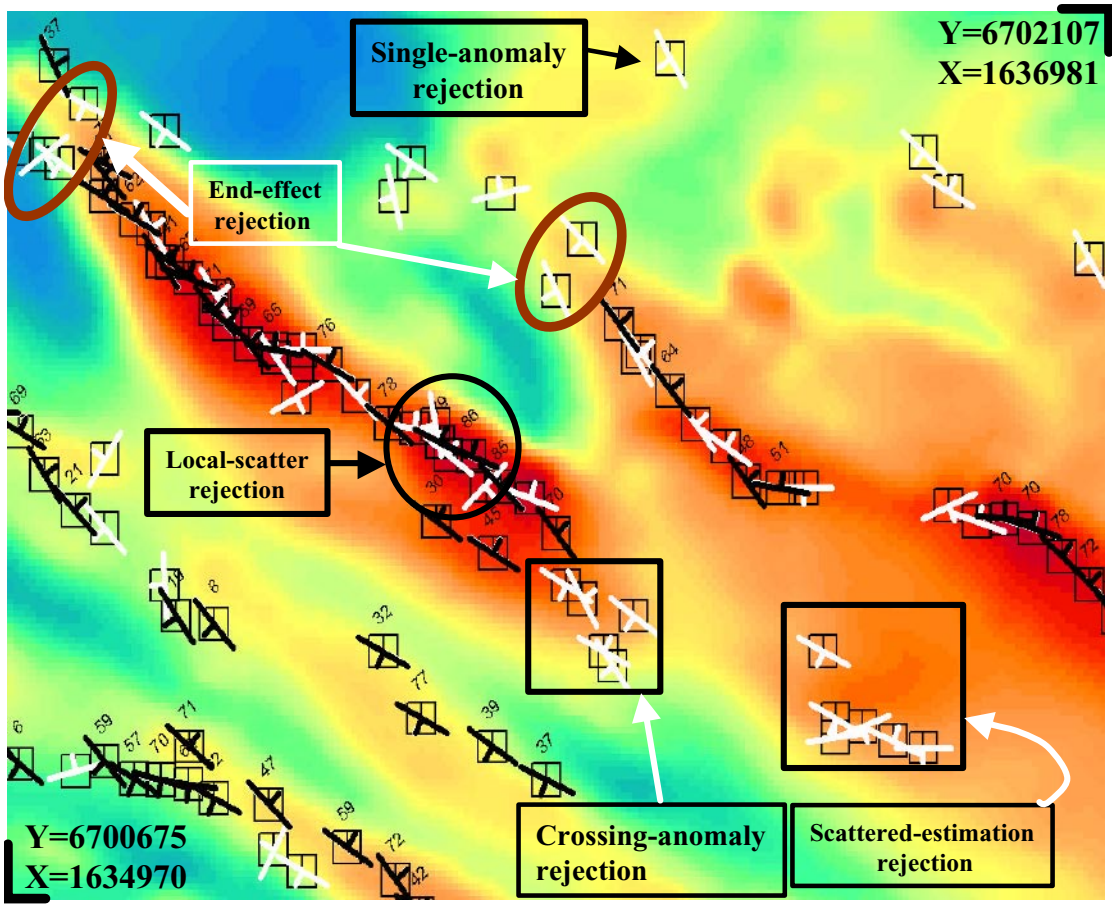

Figure 4-6. *Examples of rejection of ASM estimations based on different criteria. The white symbols show the location of raw solutions with no rejection. The black symbols show the location of selected solutions. Note that at these locations the black symbols are printed on top of the white symbols. Total magnetic field anomaly in colur (positive anomalies red, negative anomalies blue).*

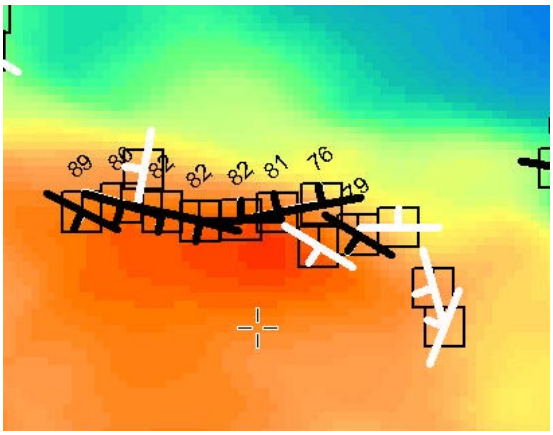

Figure 4-7. *Example of nearly vertical anomalies with scattered dip solutions. See Figure 4-6 and text for explanation.*

4.1.4 On the derivative and estimation of contact source parameters

The derivative of the magnetic field anomaly from a contact resembles the one from an infinite thin dike and this is the basic model used in the analytical signal technique. In order to distinguish between a contact and a dike, the anomaly pattern and the width-to-depth ratio found from the analytical signal of the field (not the field derivative) can be used. Higher ratios may infer contacts.

In Figure 4-8 an example of source parameter estimation shows that the estimated dips may point to opposite directions. In such circumstances the trend of magnetic field is a good measure to select the correct solution. In this example, the signature of the anomaly resembles more a contact than a dike. Therefore the estimated dips with the first derivative are more acceptable.

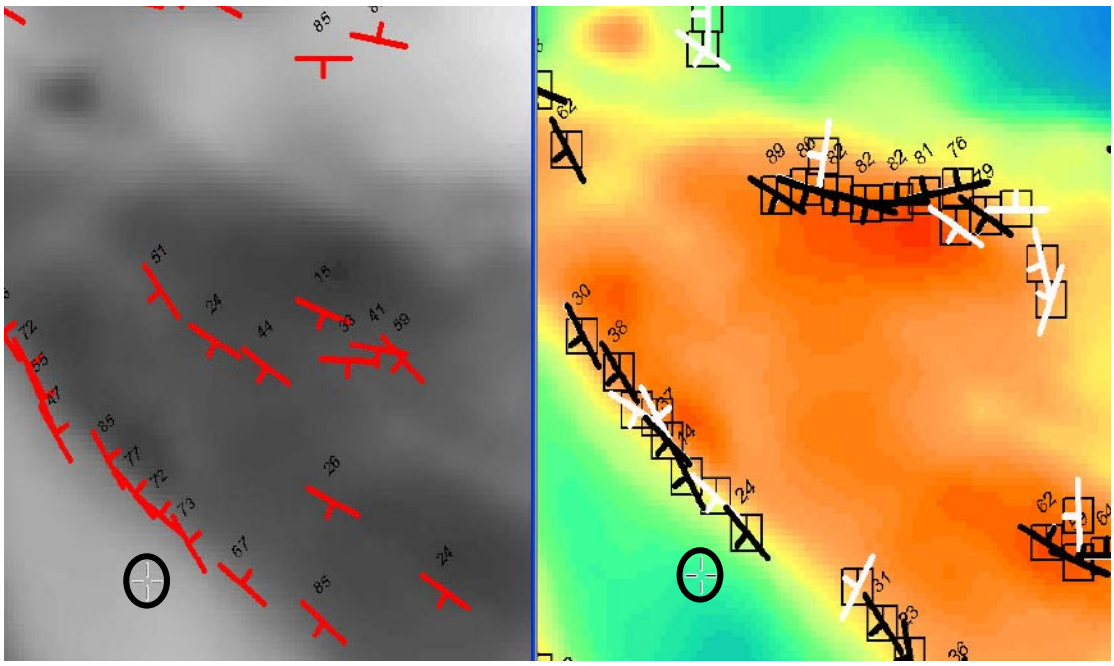

Figure 4-8. *A comparison between the estimated dips with analytical signal (right) and its 1st horizontal derivative (left). The ellipse indicates the same point in the figures. See Figure 4-1 and text for explanation. Total magnetic fied anomali in grey scale (left) and colour (right).*

4.2 Euler deconvolution

Results of processing with the Euler deconvolution

The data shown in Figure 4-1 have also been used to test the Euler deconvolution (ED) method. A structural index (SI) of 0 and a 3×3 window (50 m grid cell size) was selected to find the location of the structures and to analyse the corresponding width. Figure 4-9 shows the estimated depth to the magnetic contacts.

The locations are very well resolved. The depth estimates from the magnetic contact (structural index = 0) in ED are scattered and somewhat underestimated.

Figure 4-10 shows the map of synthetic magnetic anomalies at the crossing point of structures 1 and 3. The real depth for bodies 1 and 3 is 90 m and 200 m, respectively. The deepest solutions are closest to the true values. The width is overestimated by the ED method using a grid cell size of 50 m and SI = 0. Using a 10 m grid cell size would improve the accuracy.

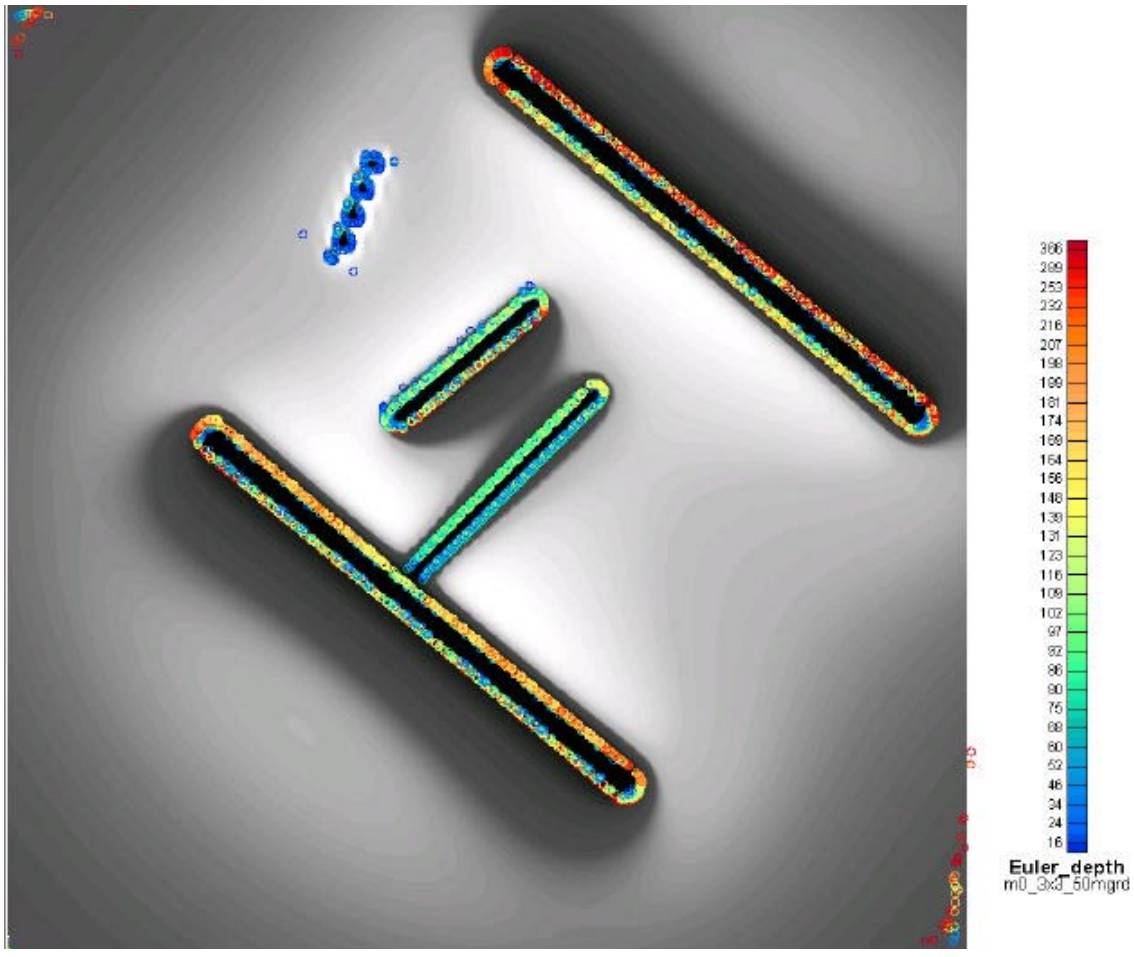

Figure 4-9. *Euler deconvolution estimates superimposed on the synthetic anomaly magnetic field. The background magnetic field is shown with an anti-grey colour scale.*

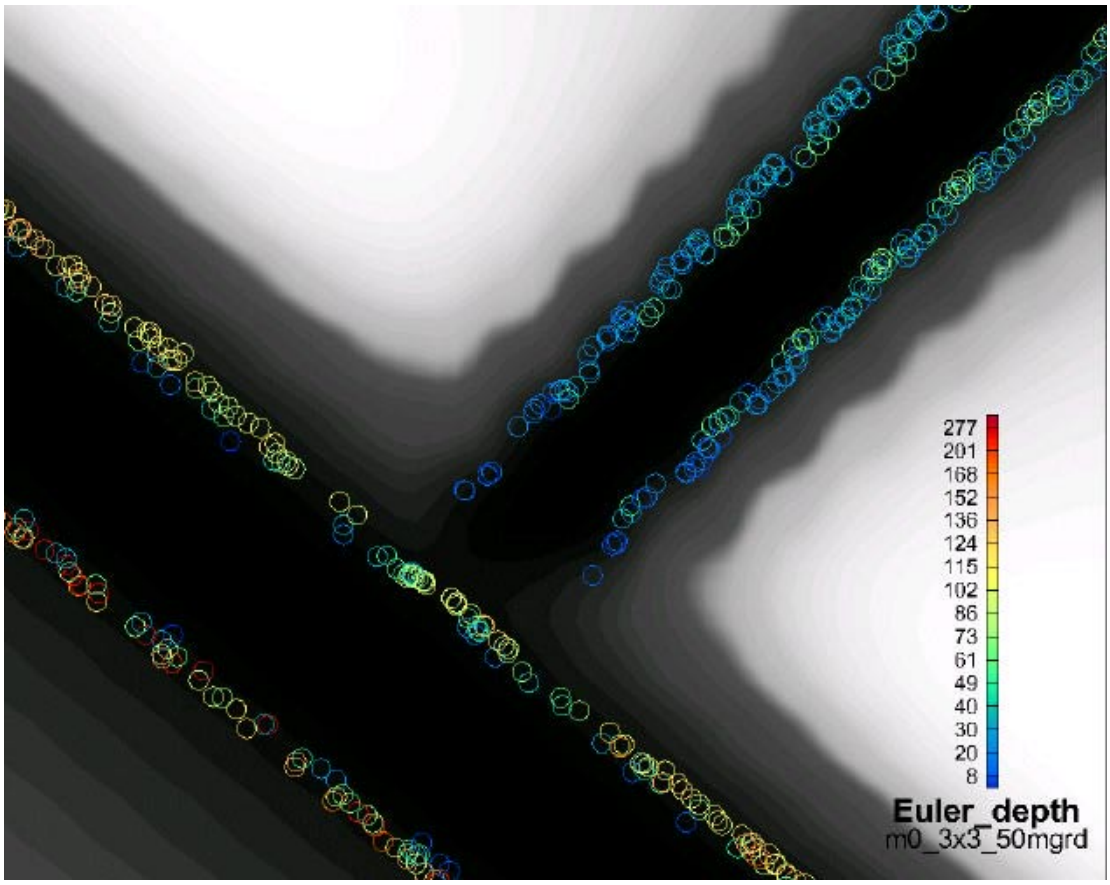

Figure 4-10. *Euler deconvolution estimates superimposed on the synthetic anomaly magnetic field, detail. The background magnetic field is shown with an anti-grey colour scale.*

Figure 4-11 illustrates the Euler solutions with a SI=1 (magnetic dyke). The window used is 10×10 (50 m grid cell). The grid quality is somewhat improved by using a linear interpolation method developed by /Bastani et al. 2002/. The depths to the top of the synthetic bodies are well reproduced by the Euler deconvolution. The width of body number 3 is 400 m which means that a 500 m×500 m window is rather small, but it is an optimised choice when the dataset contains anomalies of different sizes. A more confusing feature is the discrepancy in the depth solutions for bodies 3 and 4 which have the same dimensions although different dip directions. There are also some fragmented artefacts at the end points. Some scattered deep solutions occur at locations far away from the structures. They reveal artificial structures that may be due to the interference between the neighbouring structures. There are some artefacts seen around structure 5 although an improved grid has been used.

Figure 4-12 shows, in detail, the Euler solutions at the crossing point between anomaly 1 and 3. There are still some artificial dykes as a result of interference at the crossing point. The depth to the top of structure 3 (real depth is 200 m) is mostly overestimated. The solutions above body number1 (true depth is 90 m) are well estimated and they show small variation near the crossing point with body number 3. The depth solutions for body number 3 are also biased towards shallower estimates due to influence from body number 1 at the crossing point.

The negative contact anomaly caused by body number 3 affects the Euler solutions for body number 1 with a bias towards deeper solutions in that area. The artefacts are the effects of the 500×500 m window used in the Euler processing. In real cases it is very difficult and time-consuming procedure to distinguish and eliminate such artefacts.

The quality of the grid plays an important role in ED. The grids used in Figure 4-9 and 4-10 are made by gridding (minimum curvature) the raw data without any a priori processing. The grids shown in Figure 4-11 and 4-12 are based on data processed by the linear interpolation method developed by /Bastani et al. 2002/. The difference between the quality of the grids is noticeable. This difference also affects the Euler solutions in which less scattered and more accurate results are obtained when the pre-processed data are used.

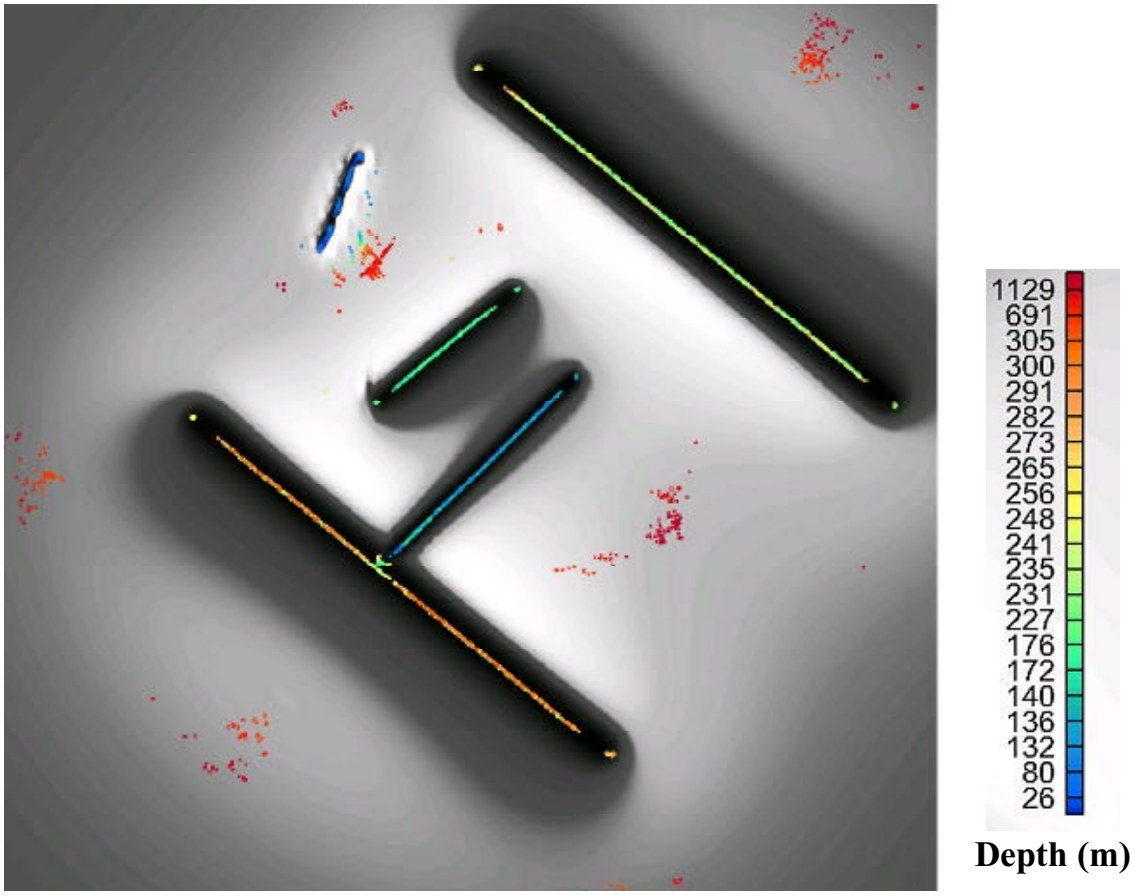

Figure 4-11. *Solutions from the Euler deconvolution, SI =1 (magnetic dyke), superimposed on the synthetic anomaly magnetic field. The background magnetic field is shown with an anti-grey colour scale.*

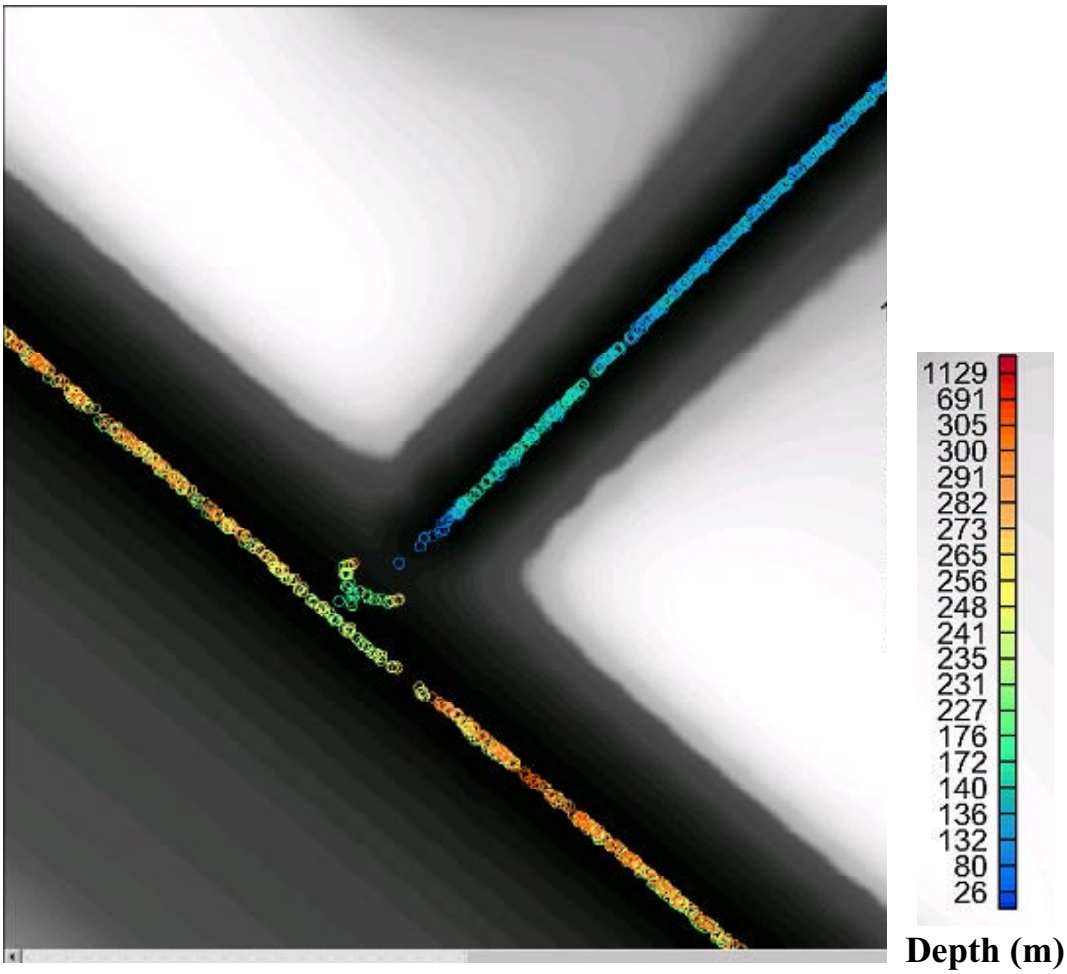

Figure 4-12. *Euler deconvolution, SI = 1 which corresponds to a magnetic dyke, on synthetic data gridded with an improved interpolation technique /Bastani et al. 2002/. The background magnetic field is shown with an anti-grey colour scale.*

4.3 Comparison with field and laboratory data

4.3.1 Correlation between the ASM solutions, the field data and the laboratory observations

Five sub-areas, areas 1 to 5, have been selected to compare the estimated strike and dip inferred from the airborne survey data and the laboratory measurements on oriented outcrop samples /Mattsson et al. 2002, Figure 5-7/. Figure 4-13 shows both the estimated ASM strikes/dips and the laboratory results. The laboratory results shown belong to rock group A (supracrustal rocks) and B (Ultramafic, mafic, intermediate and quartz-rich felsic meta-intrusive rocks). The rock group terminology has been defined by SKB for the Forsmark area.

In area 1, the laboratory measurements show a shallowly dipping (32° SSW) structure. Close to this observation point, three ASM solutions show a shallowly dipping structure (31°, 23°, 36° WSW). The estimated strikes differ within a few degrees.

In area 2, the laboratory measurements of samples from two sites show moderately dipping magnetic fabrics (62°and 55° SSW). The ASM solutions show also a moderately to steeply dipping structure in almost the same direction (62°, 80°, 82° and 90° SSW) close to the 62° location and a shallowly to moderately dipping structure (17°, 27°, 30°, 31° and 32° SSW) close to the 55° location.

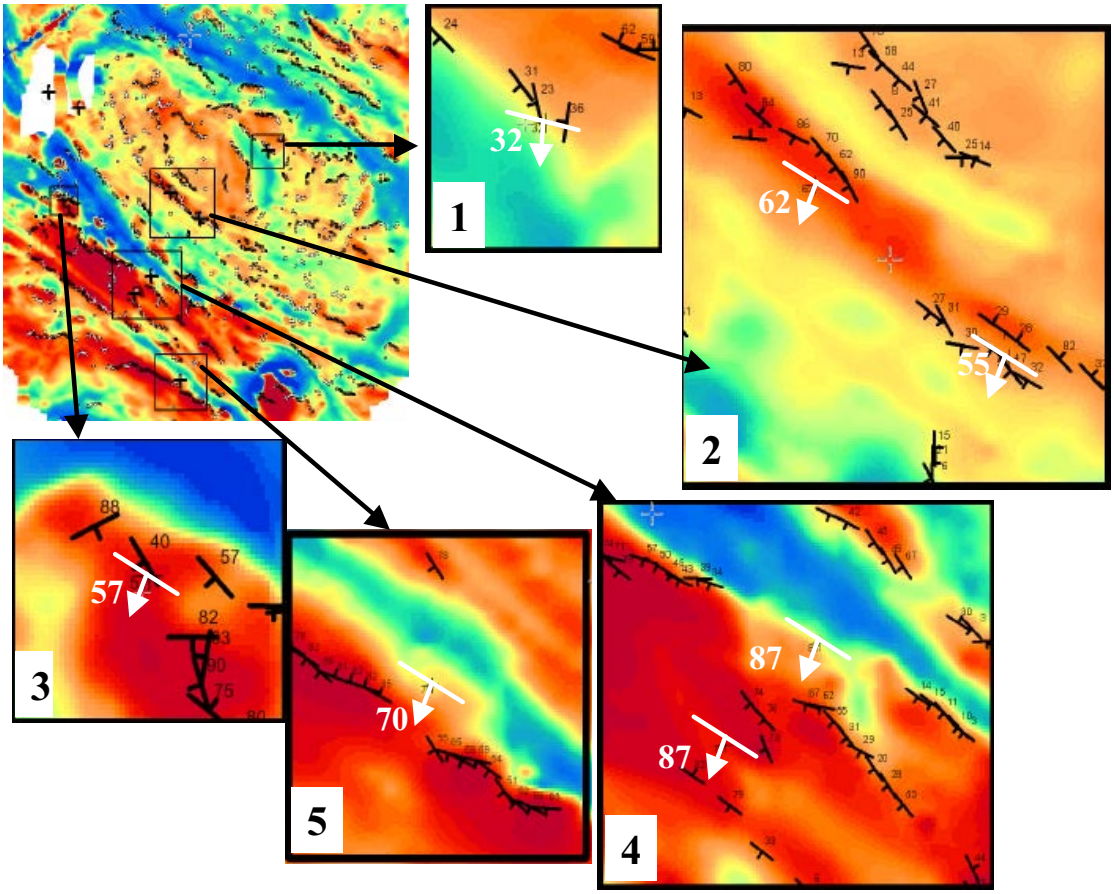

Figure 4-13. *Comparison between the ASM solutions and the results of laboratory measurements of magnetic anisotropy. The black symbols show the ASM solutions and the white symbols the laboratory results. Locations of the outcrop samples have been picked from Figure 5-7 in / Mattsson et al. 2002/ and might be slightly different from the real locations.*

In the third area the "laboratory" dip is equal to 57°. The ASM solutions are more scattered compared to areas 1 and 2 and vary between 40° and 90° with varying strikes.

In area 4, the laboratory-measured dips (at 2 locations) indicate a steeply (87°) towards SSW dipping magnetic fabric. The general trend of the estimated ASM strikes in the area close to these localities corresponds well. 90% of the estimated dip directions are in the same direction (SSW) although close to one location there is one estimated dip to the opposite direction. The ASM estimated dips vary between 55° to 79° at a maximum distance of about 200 m from the sampling locations. Shallower dips with the same directions are however also found in the same area (see Figure 4-13).

In area 5, the result (70° SSW) from the only site sampled for laboratory measurements correlates very well with the ASM solutions that vary between 55° to 88° SSW. However, there are some steeply dipping solutions to the west of reference point with an opposite direction (81°–85° NNE). This difference may originate from noise, remanent magnetisation or three-dimensionality.

4.3.2 Comparison between ASM, Euler deconvolution and the in situ measured structural data

In this section the estimated ASM and Euler deconvolution parameters have been compared with field structural measurements from /Stephens et al. 2003/.

Figure 4-14a–c shows the estimated dips and strikes from the processing of the ASM (positive anomaly signature), the ASM (negative signature) and the horizontal derivative of the AS (positive signature), respectively. In Figure 4-14d, field observations of dips and strikes of the ductile foliation are displayed.

The area marked by white rectangle (c 3.5 km × 2 km) in Figure 4-14 was selected for more detailed analyses (Figure 4-15). In the upper left corner the strike and dip based on the positive magnetic anomaly is shown and in the lower left corner field measurements of the strike and dip of the foliation. The yellow symbols represent vertical foliation. Upper and lower right corners show the strikes and dips from the ASM processing based on the positive derivative of the magnetic anomalies, respectively. Also the Euler solutions have been added.

The data set Grid_Mag_Euler_0_3×3_10mgrd_ns, containing the Euler solutions is shown in Figures 4-16 and 4-17. The area is the same detailed area as marked in Figure 4-14. The depth from the ground level to the magnetic contact is also displayed. The solutions provide some information on depths that can be interpreted as the relative soil thickness. In this example, the very small window used (3×3 with a 10 m grid cell size) encompasses mostly the effects of shallow structures in the processing. The absolute depth in these solutions must be evaluated point to point. The outcrops are marked with large blue symbols.

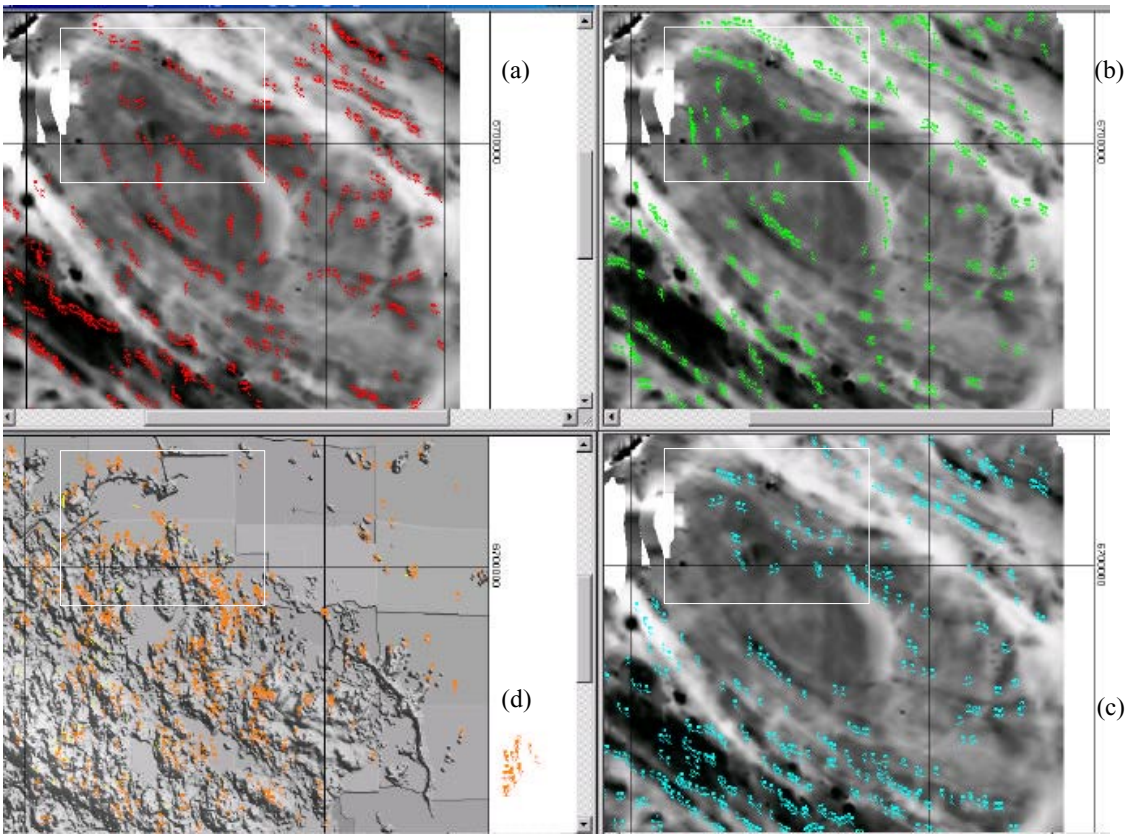

Figure 4-14. *Location of the area, white rectangle, presented in detail in Figure 4-15 a-c, showing estimated dip and strike from ASM processing based on a) the analytic signal (positive anomaly signature), b) the analytical signal (negative anomaly signature) c) the horizontal derivative of the analytic signal (positive anomaly signature) d) field observations. The dips and strikes are superimposed on the magnetic anomaly map shown with an anti-gray colour scale (a-c) and elevation data shown with a shaded gray scale (d).*

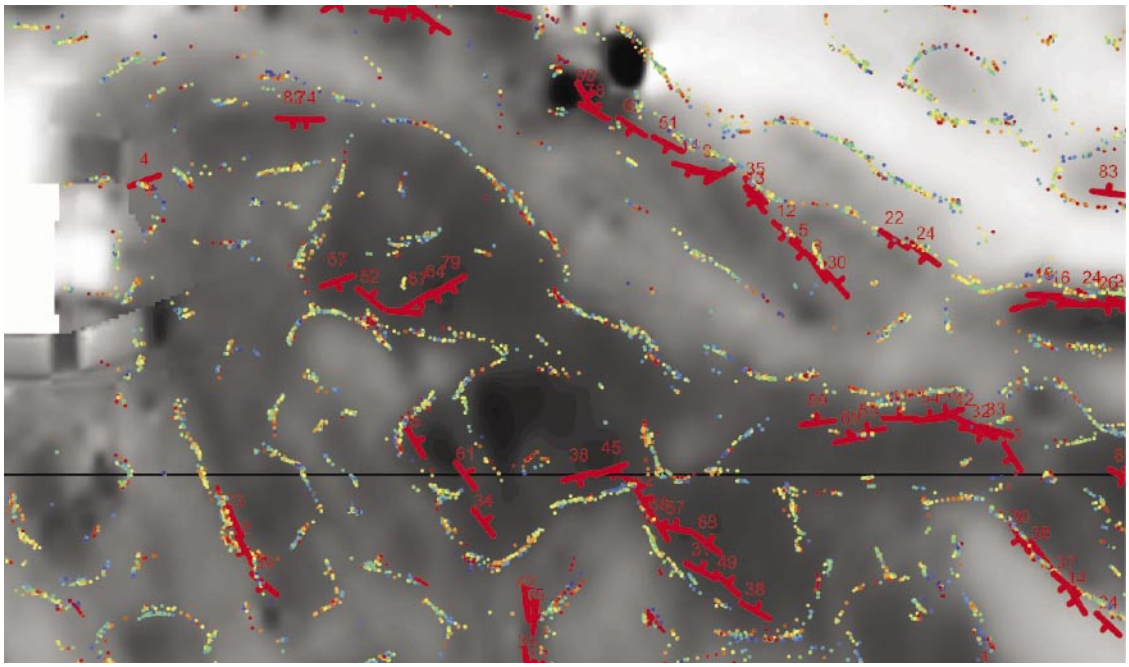

a)

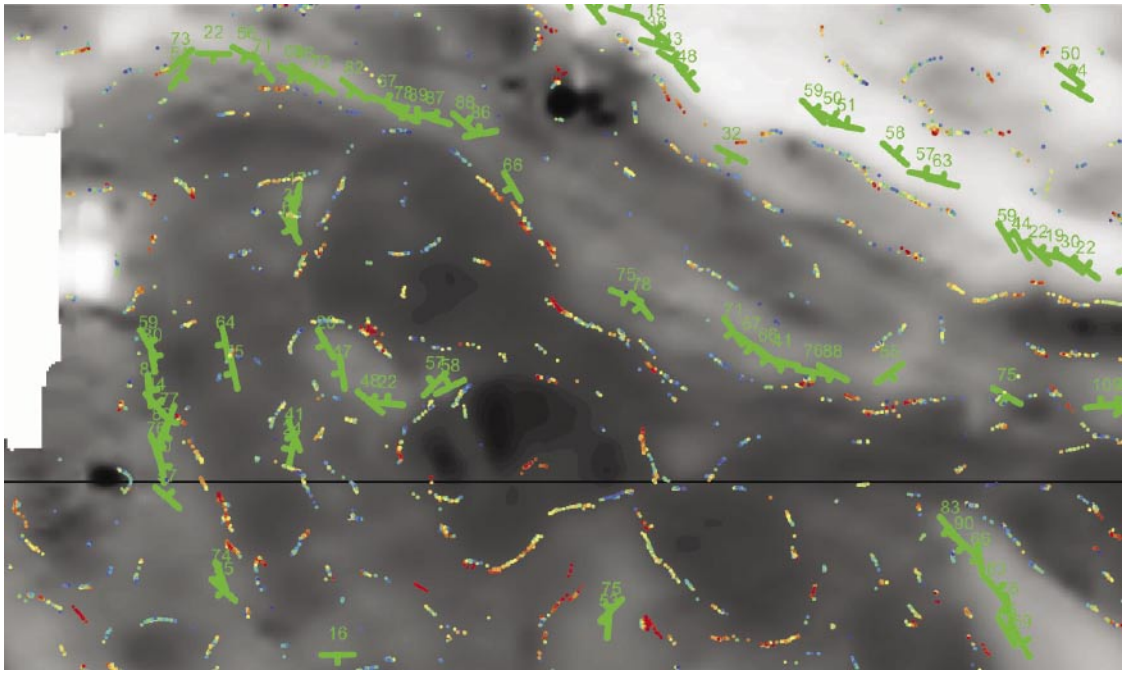

b)

Figure 4-15 a, b. *Detail of the area marked by the white rectangle in Figure 4-14. The area is c 3.5 km × 2 km. Estimated dip and strike from ASM processing based on a) the analytic signal (positive anomaly signature), b) the analytical signal (negative anomaly signature). The dips and strikes are superimposed on the magnetic anomaly map shown with an anti-gray colour. Data from Euler deconvolution is added as small dots (depth scale as in Figure 4-16).*

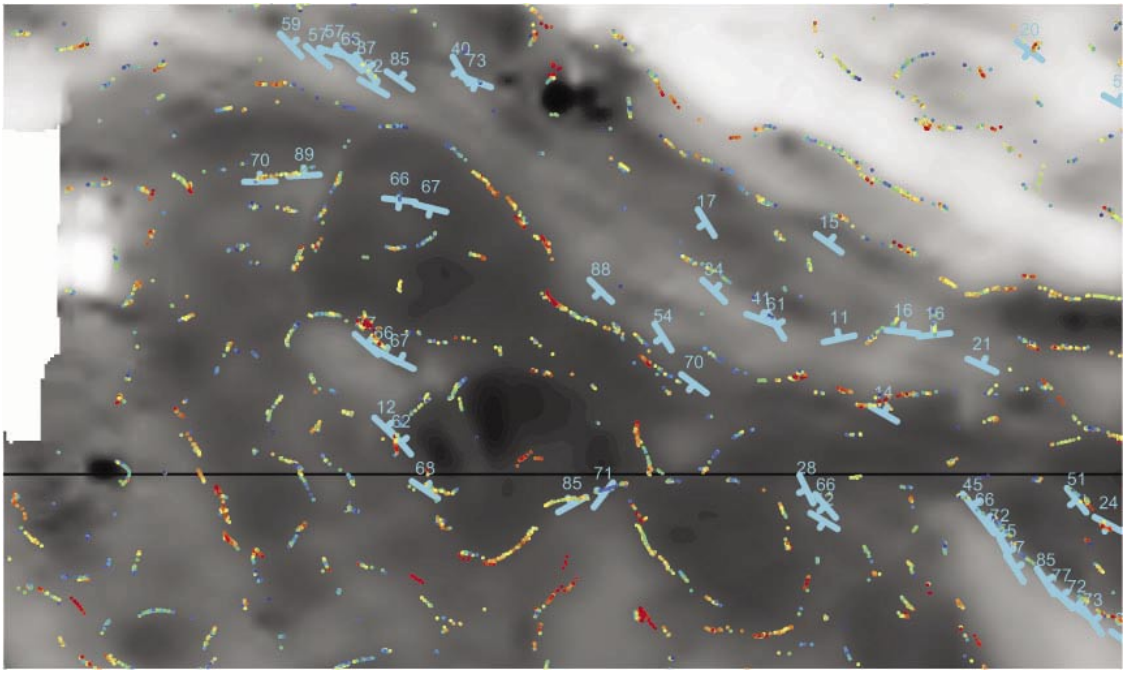

c)

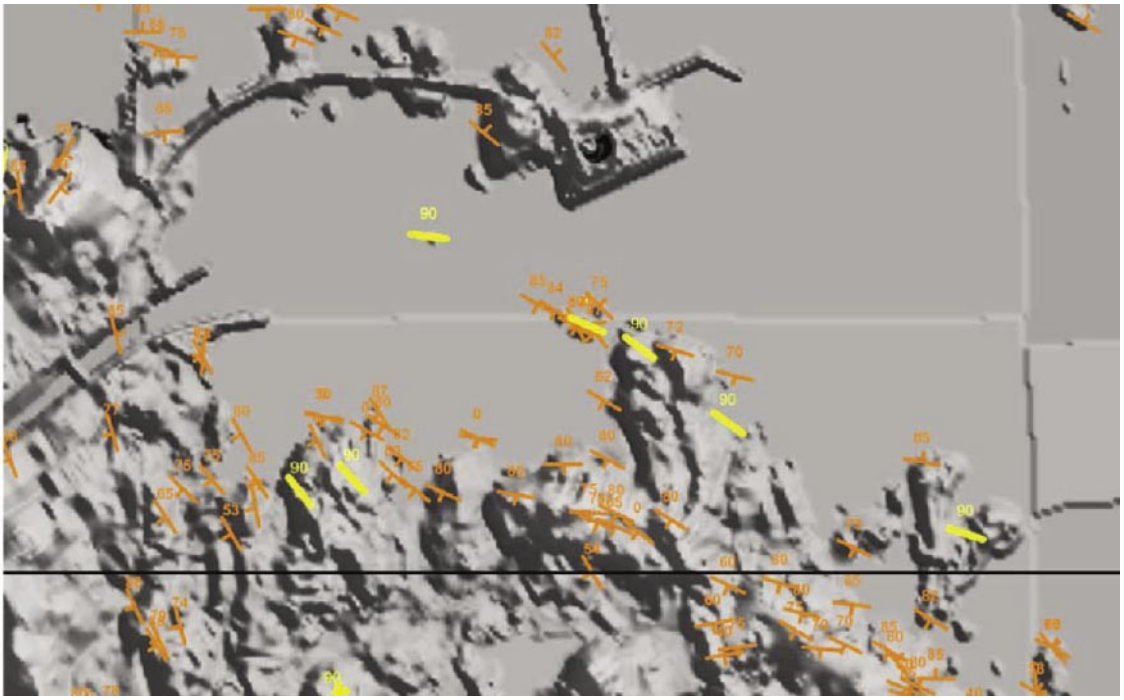

d)

Figure 4-15 c, d. *Detail of the area marked by the white rectangle in Figure 4-14. The area is c 3.5 km × 2 km. Estimated dip and strike from ASM processing based on c) the horizontal derivative of the analytic signal (positive anomaly signature) and d) field observations. The dips and strikes are superimposed on the magnetic anomaly map shown with an anti-gray colour scale (c) and elevation data shown with a shaded gray scale (d). Data from Euler deconvolution is added as dots (c only, (depth scale as in Figure 4-16)).*

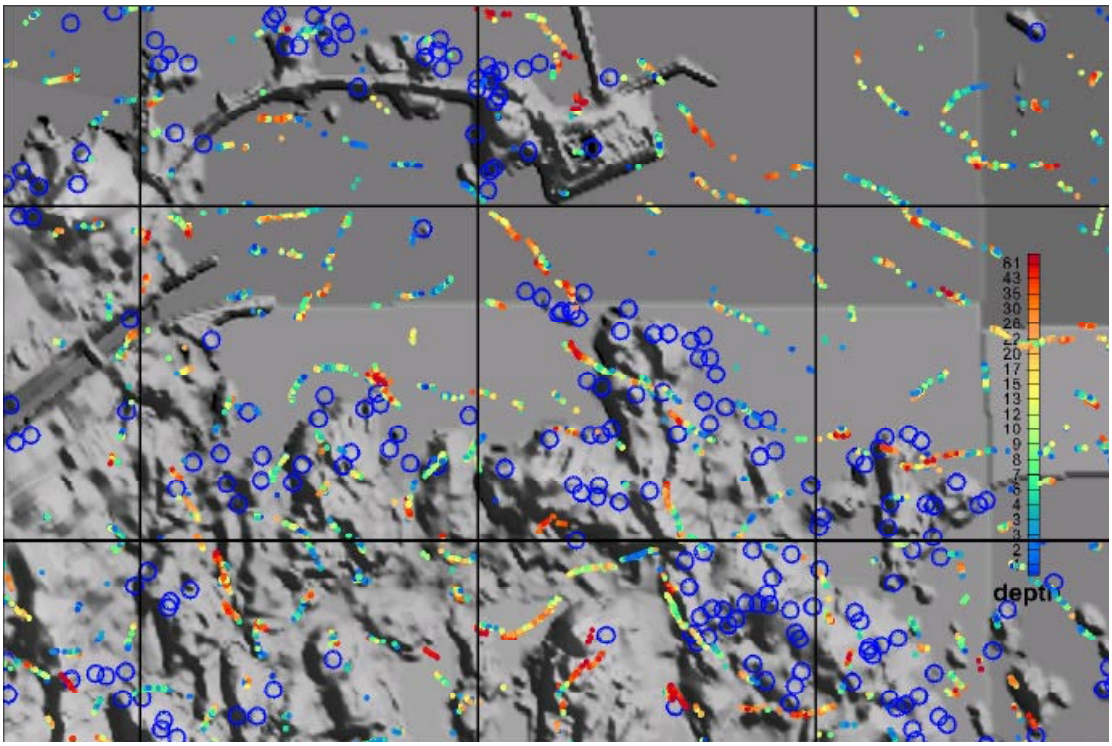

Figur 4-16. *Solutions from Euler deconvolution, depth from the ground surface to the magnetic contact. Blue symbols show outcrops superimposed on the elevation data in shaded grey scale.*

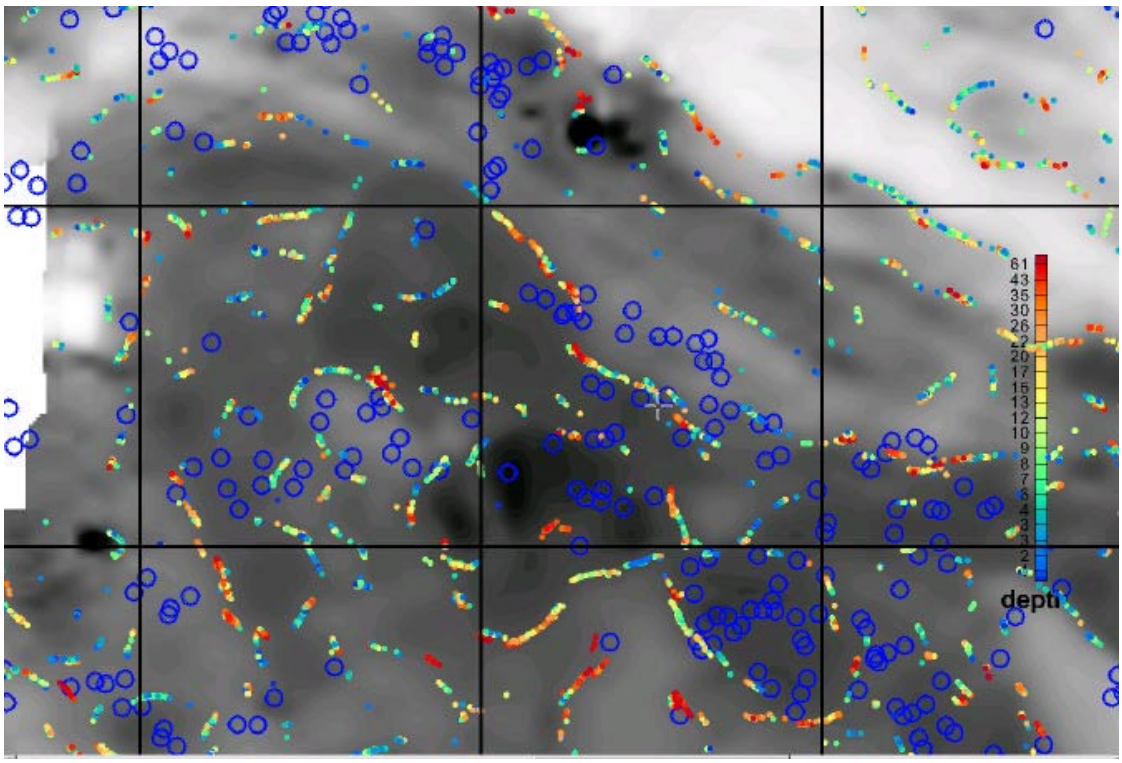

Figur 4-17. *Solutions from Euler deconvolution, depth from the ground surface to the magnetic contact. Blue symbols show outcrops superimposed on the total magnetic field in anti-grey colour scale.*

5 Important results and conclusions

5.1 Concluding remarks

The analytical signal method (ASM) is a very fast method to evaluate the source parameters of two-dimensional magnetic anomalies. The method can be used as a powerful tool to pinpoint the interesting areas as well as to gain an overall knowledge about the geometry and orientation of causative structures in a study area.

By comparing the estimated and the real source parameters for a given synthetic model the capabilities and limitations of the method have been analyzed. The modelling showed that the method is capable to estimate the source parameters (dip, depth, width and strike) for elongated structures. In order to control the estimated depths, the estimations from the ASM processing have been compared with the results from the Euler deconvolution method. The results show that the methods are complementary and provide useful structural information. The estimated depths can also be used to trace the depth variations in the area (determination of depth gradient).

In practice, the source parameters found must be interpreted with a special care since there are several fundamental assumptions made. These assumptions may not always be fully relevant and the measured data may also contain noise and artificial anomalies not related to the geological setting. The source parameters must therefore be carefully examined and irrelevant solutions rejected. Within the present test area, c 50% of the solutions was rejected. The comparison between the estimated dips and strikes remaining and the results from field and laboratory measurements showed a reasonable correlation.

The results from the Euler deconvolution of the synthetic data showed good results. Apart from violations of the assumed 2D conditions the homogeneity of the depth solutions is also dependent of the quality of the grid. For measured data the deviation from the assumed model gives greater disturbances in the solution pattern. The discrimination of the many solutions is here done mainly spatially.

The Euler solutions between flight lines are based on gridded information (magnetic field and ground clearance) of which the ground clearance is not well suited for gridding. As long as the ground clearance variation from one flight line to the other is small, the gridding however yields usable information.

5.2 How to use the interpretation results

The ASM and ED results contain many details about the magnetic structures in the area and some further analysis using both data sets would improve the interpretation. It can however hardly be expected to find an exclusive method that will meet every interpretation challenge. Instead all available tools must be combined.

The results of the ASM and ED processing presented in this report should therefore be used together with other information, e.g. geophysical interpretation of airborne and ground and borehole surveys, information from geological mapping of outcrops and drill cores.

Used with caution, the ASM and ED results can provide important support to the modelling of rocks and deformation zones. The next step could be to conduct a detailed comparison between the estimated source parameters and the models found by forward and inverse modelling of the existing geophysical and geological data.

Figures 5-1 and 5-2 show some ASM and ED results from a sub-area just southwest of the Forsmark candidate area. The results contain information on the inferred lineaments (Figure 5-1) and depth to magnetic sources (Figure 5-2). The results support the 3D-modelling of rocks and structures when combined with for example mapping and drilling information. It should be noted that the results presented in Figures 5-1 and 5-2 also should be combined with other ASM/ED results (e.g. Euler solutions for other structural indices and processing windows).

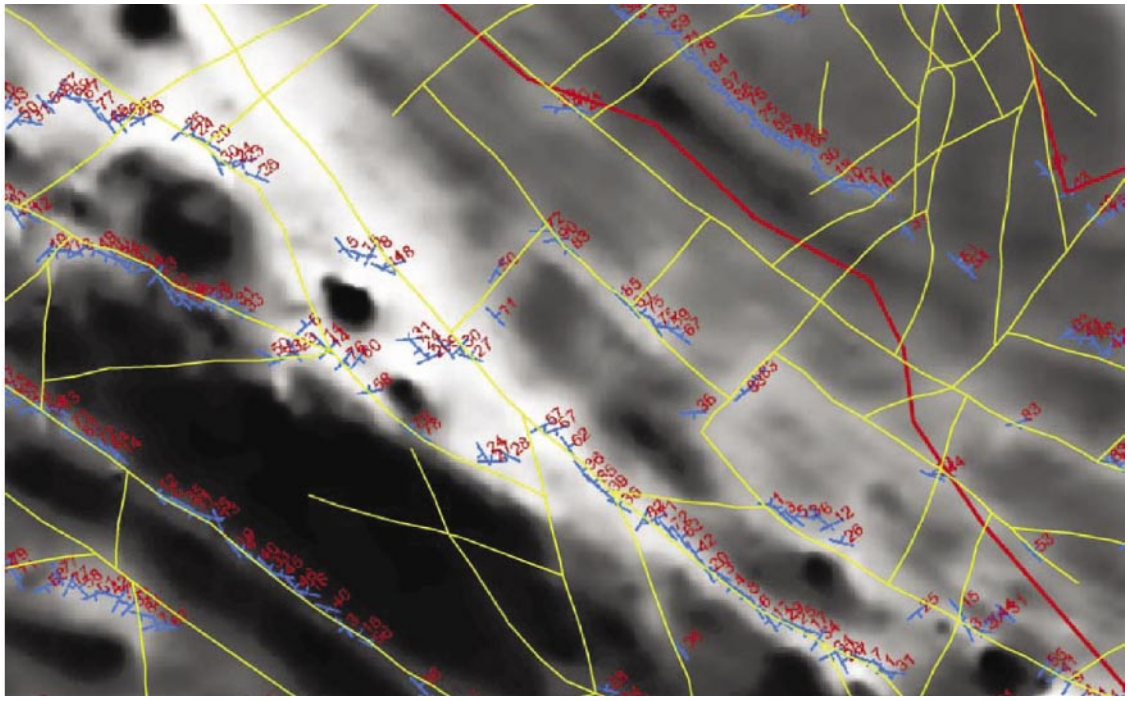

Figure 5-1. *Estimated ASM dips and strikes using the NS data and magnetic anomalies with negative signature. Excerpt from Figure 2-5. Interpreted lineaments /Isaksson et al. 2004/ in yellow. See text for explanation. The area shown is situated along the south-western border (solid red line) of the Forsmark candidate area.*

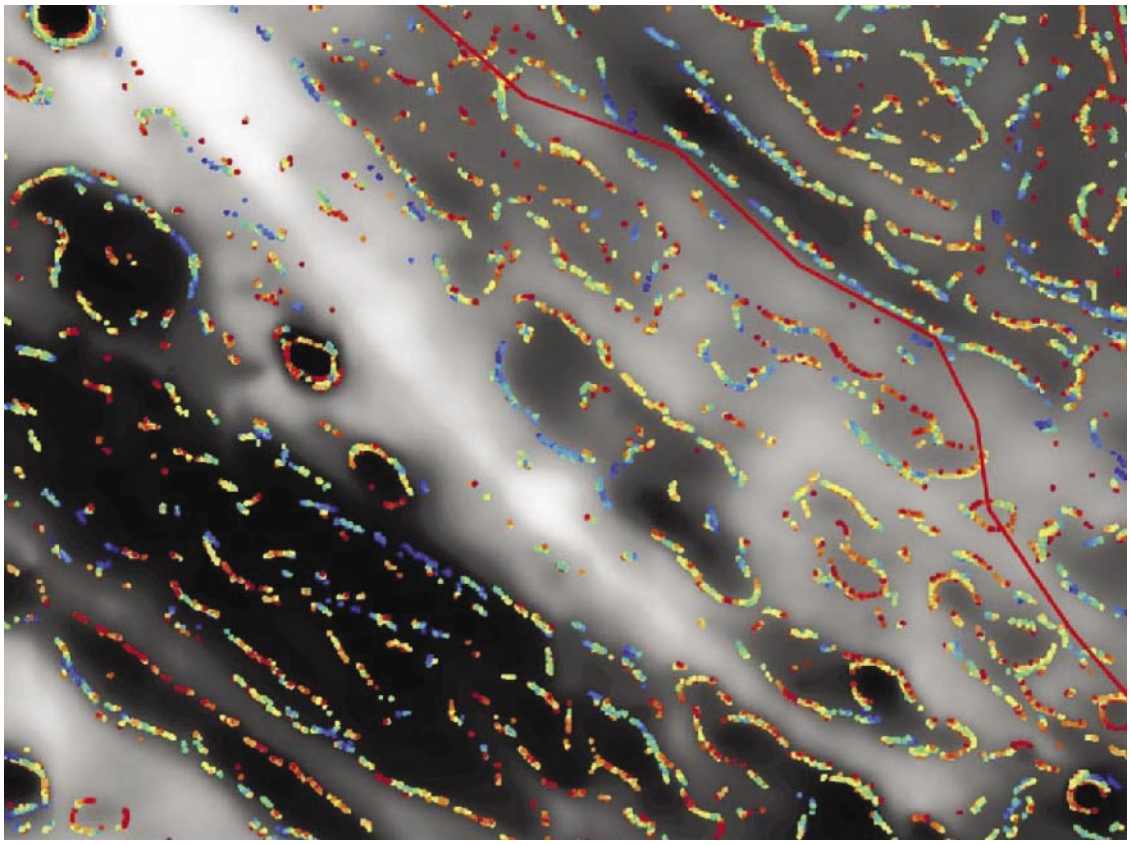

Figure 5-2. *Euler solutions (NS survey, 10 m grid, 3×3 grid cells window, structural index = 0). Excerpt from Figure 3-1. See Figure 3-1 for legend and text for explanation. The area shown is situated along the south-western border (solid red line) of the Forsmark candidate area.*

6 Data delivery

The data delivery includes a considerable number of XYZ- and image files in two zip-files on a CD. The zip-files contain results from the analytic signal technique and Euler deconvolution, respectively. The following sections document the file nomenclature and the structure of the XYZ-files. Listing of the delivered files is also provided.

6.1 Analytic signal

File nomenclature

The numerical results (estimated source parameters, e.g. dip and depth) are stored in ASCII XYZ-files with a name showing the processing specifications. All the file names begin with “SelArea_Dip_Depth_Width_Strike_” describing, for the selected area which has been processed, the results in the order they reside in the data files. The second part of the name presents the magnetic anomaly used to calculate the source parameters. For example “ NegAnomali “ means that the estimated parameters belong to an anomaly with a negative signature. The last part shows the flight-direction (EW, NS or EW and NS combined).

Example of file name: SelArea_Dip_Depth_Width_Strike_PosAnomali_Der_ew.XYZ

The image files, in AreView tiff format, are stored in files with a name representing the contents. For example the file named “Grid_Mag_Negative_ew+ns_Depth.tif ” contains an image of gridded magnetic field with the superimposed depth estimation of anomalies with a negative signature and combined “ew+ns “ flight-directions. Image files containing the estimated parameters with no grey-scaled magnetic field grid follow the same naming convention but the file name does not, consequently, include “Grid_Mag”.

Example of file names:
Grid_Mag_Negative_ew+ns_Depth.tfw
Negative_ew+ns_Depth.tfw

XYZ file structure

The XYZ-files contain the following columns:
X: Easting(RT90) in metres
Y: Northing(RT90) in metres
Dip: Degrees from horisontal
Depth: Meters from ground surface
Width: Metres
Strike: Degrees from north (RT90)
Ratio: Width/Depth (dimensionless)

Files delivered

XYZ-files, (combined flight data):

SelArea_Dip_Depth_Width_Strike_NegAnomali_ew+ns.XYZ
SelArea_Dip_Depth_Width_Strike_PosAnomali_Der_ew+ns.XYZ
SelArea_Dip_Depth_Width_Strike_PosAnomali_ew+ns.XYZ

XYZ-files, refined parameters after interpretation:

SelArea_Interp_Dip_Depth_Width_Strike_NegAnomali_ew+ns.XYZ
SelArea_Interp_Dip_Depth_Width_Strike_PosAnomali_Der_ew+ns.XYZ
SelArea_Interp_Dip_Depth_Width_Strike_PosAnomali_ew+ns.XYZ

Tiff-files (estimated parameters superimposed on magnetic grid):

Grid_Mag_Negative_ew_DipStrike.tfw
Grid_Mag_Negative_ew_DipStrike.tif
Grid_Mag_Negative_ns_DipStrike.tfw
Grid_Mag_Negative_ns_DipStrike.tif
Grid_Mag_PositiveDer_ew_DipStrike.tfw
Grid_Mag_PositiveDer_ew_DipStrike.tif
Grid_Mag_PositiveDer_ns_DipStrike.tfw
Grid_Mag_PositiveDer_ns_DipStrike.tif
Grid_Mag_Positive_ew_DipStrike.tfw
Grid_Mag_Positive_ew_DipStrike.tif
Grid_Mag_Positive_ns_DipStrike.tfw
Grid_Mag_Positive_ns_DipStrike.tif

Tiff-files (estimated parameters only):

Interpreted_Negative_ew+ns_DipStrike_FinalVersion.tfw
Interpreted_Negative_ew+ns_DipStrike_FinalVersion.tif
Interpreted_PositiveDer_ew+ns_DipStrike_FinalVersion.tfw
Interpreted_PositiveDer_ew+ns_DipStrike_FinalVersion.tif
Interpreted_Positive_ew+ns_DipStrike_FinalVersion.tfw
Interpreted_Positive_ew+ns_DipStrike_FinalVersion.tif
Negative_ew+ns_DipStrike_FinalVersion.tfw
Negative_ew+ns_DipStrike_FinalVersion.tif
PositiveDer_ew+ns_DipStrike_FinalVersion.tfw
PositiveDer_ew+ns_DipStrike_FinalVersion.tif
Positive_ew+ns_DipStrike_FinalVersion.tfw
Positive_ew+ns_DipStrike_FinalVersion.tif
Negative_ns_DipStrike.tfw
Negative_ns_DipStrike.tif
Negative_ew_DipStrike.tfw
Negative_ew_DipStrike.tif

PositiveDer_ew_DipStrike.tfw
PositiveDer_ew_DipStrike.tif
PositiveDer_ns_DipStrike.tfw
PositiveDer_ns_DipStrike.tif
Positive_ew_DipStrike.tfw
Positive_ew_DipStrike.tif
Positive_ns_DipStrike.tfw
Positive_ns_DipStrike.tif

6.2 Euler deconvolution

File nomenclature

The numerical results (estimated source parameters, e.g. dip and depth) are stored in ASCII XYZ-files with a name showing the processing specifications. The naming convention is Grid_Mag_Euler_structural index_window size_grid cell size_flight direction_ upward continuation level.

Example of file name:
Grid_Mag_Euler_0_3x3_100mgrd_up500_ns.xyz

The file above hence contains processing results with the following parameters applied:
Structural index = 0
Window size = 3×3 grid cells
Grid cell size = 100 m
Data is upward continued 500 m and the flight lines are trending NS.

The image files, in AreView tiff format, are stored in files with a name representing the contents. For example, the file named "Grid_Mag_Euler_0_20x20_100mgrd_up1000_ greygrdup1000_ew.tif " contains an image of the 1,000 m upward continued magnetic field with the superimposed Euler solutions (structural index = 0, window size 20x20 grid cells, grid cell size = 100 m) based on EW trending survey lines.

Image files containing the estimated parameters with no grey-scaled magnetic field grid follow the same naming convention but the file name does not, consequently, include the definition of the background grid (greygrd, greygrdup1000up etc).

Finally, the file "surface_related" contains Euler solutions related to the ground level and the file "surface_corr" only the solutions below the ground level (solutions above ground level are rejected).

XYZ file structure

The XYZ-files cointain the following columns, including a few new columns are added to the output file from the Geosoft Euler 3D Deconvolution program module:

X_Euler:	Easting(RT90) in metres
Y_Euler:	Northing(RT90) in metres
Depth:	Depth (m) under ground surface
Backgrnd:	Solution base level
WndSize:	Size of search window (m)

Dz:	Percentage depth uncertainty
Dxy:	Location uncertainty as a percentage of solution depth z
Mask:	Flag indicating whether this solution is to be plotted or not
X_Window:	X co-ordinate of the center of the search window
Y_Window:	Y co-ordinate of the center of the search window
X_Offset:	X–X_Window
Y_Offset:	Y–Y_Window
xoff_75	–75m > X_Offset < 75m
yoff_75	–75m > Y_Offset < 75m
raltm:	Radar altimeter hight (ground clearance) (m)
groundlevel:	Topographic height above sea level (m)
asl	above sea level (m)
asl_30m	asl < 30m
surface_related	asl_30m – groundlevel
surface_corr	asl_30m – groundlevel < 0 m

Files delivered

XYZ-files:

Grid_Mag_Euler_0_3x3_10mgrd_ew_surface_corr.XYZ
Grid_Mag_Euler_0_3x3_10mgrd_ns_surface_corr.XYZ
Grid_Mag_Euler_1_3x3_10mgrd_ew_surface_corr.XYZ
Grid_Mag_Euler_1_3x3_10mgrd_ns_surface_corr.XYZ
Grid_Mag_Euler_0_3x3_10mgrd_ew.xyz
Grid_Mag_Euler_0_3x3_10mgrd_ns.xyz
Grid_Mag_Euler_0_3x3_25mgrd_ew.xyz
Grid_Mag_Euler_0_3x3_25mgrd_ns.xyz
Grid_Mag_Euler_0_3x3_100mgrd_ew.xyz
Grid_Mag_Euler_0_3x3_100mgrd_ns.xyz
Grid_Mag_Euler_0_3x3_100mgrd_up500_ns.xyz
Grid_Mag_Euler_0_3x3_100mgrd_up1000_ew.xyz
Grid_Mag_Euler_0_3x3_100mgrd_up1000_ns.xyz
Grid_Mag_Euler_0_10x10_10mgrd_ew.xyz
Grid_Mag_Euler_0_10x10_100mgrd_ew.xyz
Grid_Mag_Euler_0_10x10_100mgrd_ns.xyz
Grid_Mag_Euler_0_20x20_10mgrd_ew.xyz
Grid_Mag_Euler_0_20x20_10mgrd_ns.xyz
Grid_Mag_Euler_0_20x20_25mgrd_ew.xyz
Grid_Mag_Euler_0_20x20_25mgrd_ns.xyz
Grid_Mag_Euler_0_20x20_100mgrd_up500_ns.xyz
Grid_Mag_Euler_0_20x20_100mgrd_up1000_ew.xyz
Grid_Mag_Euler_0_20x20_100mgrd_up1000_ns.xyz
Grid_Mag_Euler_1_20x20_10mgrd_ns.xyz
Grid_Mag_Euler_1_20x20_25mgrd_ew.xyz
Grid_Mag_Euler_1_20x20_25mgrd_ns.xyz
Grid_Mag_Euler_2_20x20_25mgrd_ew.xyz

Grid_Mag_Euler_2_20x20_25mgrd_ns.xyz
Grid_Mag_Euler_3_20x20_25mgrd_ew.xyz
Grid_Mag_Euler_3_20x20_25mgrd_ns.xyz
Grid_Mag_Euler_05_3x3_100mgrd_ew.xyz
Grid_Mag_Euler_05_3x3_100mgrd_ns.xyz

Tiff-files (estimated parameters superimposed on magnetic grid):

Grid_Mag_Euler_0_3x3_10mgrd_ns_greygrd.tif
Grid_Mag_Euler_0_3x3_10mgrd_ns_greygrd.tfw
Grid_Mag_Euler_0_3x3_25mgrd_ns_greygrd.tif
Grid_Mag_Euler_0_3x3_25mgrd_ns_greygrd.tfw
Grid_Mag_Euler_0_3x3_100mgrd_up500_up500greygrd_ns.tif
Grid_Mag_Euler_0_3x3_100mgrd_up500_up500greygrd_ns.tfw
Grid_Mag_Euler_0_10x10_100mgrd_ew_greygrd.tif
Grid_Mag_Euler_0_10x10_100mgrd_ew_greygrd.tfw
Grid_Mag_Euler_0_20x20_100mgrd_up1000_greygrdup1000_ew.tif
Grid_Mag_Euler_0_20x20_100mgrd_up1000_greygrdup1000_ew.tfw
Grid_Mag_Euler_05_3x3_100mgrd_ns_greygrd.tif
Grid_Mag_Euler_05_3x3_100mgrd_ns._greygrd.tfw

Tiff-files (estimated parameters only):

Grid_Mag_Euler_0_3x3_10mgrd_ew_surface_corr.tif
Grid_Mag_Euler_0_3x3_10mgrd_ew_surface_corr.tfw
Grid_Mag_Euler_0_3x3_10mgrd_ns_surface_corr.tif
Grid_Mag_Euler_0_3x3_10mgrd_ns_surface_corr.tfw
Grid_Mag_Euler_1_3x3_10mgrd_ew_surface_corr.tif
Grid_Mag_Euler_1_3x3_10mgrd_ew_surface_corr.tfw
Grid_Mag_Euler_1_3x3_10mgrd_ns_surface_corr.tif
Grid_Mag_Euler_1_3x3_10mgrd_ns_surface_corr.tfw
Grid_Mag_Euler_0_3x3_10mgrd_ew.tif
Grid_Mag_Euler_0_3x3_10mgrd_ew.tfw
Grid_Mag_Euler_0_3x3_10mgrd_ns.tif
Grid_Mag_Euler_0_3x3_10mgrd_ns.tfw
Grid_Mag_Euler_0_3x3_25mgrd_ew.tif
Grid_Mag_Euler_0_3x3_25mgrd_ew.tfw
Grid_Mag_Euler_0_3x3_25mgrd_ns.tif
Grid_Mag_Euler_0_3x3_25mgrd_ns.tfw
Grid_Mag_Euler_0_3x3_100mgrd_ew.tif
Grid_Mag_Euler_0_3x3_100mgrd_ew.tfw
Grid_Mag_Euler_0_3x3_100mgrd_ns.tif
Grid_Mag_Euler_0_3x3_100mgrd_ns.tfw
Grid_Mag_Euler_0_3x3_100mgrd_up500_ns.tif
Grid_Mag_Euler_0_3x3_100mgrd_up500_ns.tfw
Grid_Mag_Euler_0_3x3_100mgrd_up500_ew.tif

Grid_Mag_Euler_0_3x3_100mgrd_up500_ew.tfw
Grid_Mag_Euler_0_3x3_100mgrd_up1000_ew.tif
Grid_Mag_Euler_0_3x3_100mgrd_up1000_ew.tfw
Grid_Mag_Euler_0_3x3_100mgrd_up1000_ns.tif
Grid_Mag_Euler_0_3x3_100mgrd_up1000_ns.tfw
Grid_Mag_Euler_0_10x10_10mgrd_ew.tif
Grid_Mag_Euler_0_10x10_10mgrd_ew.tfw
Grid_Mag_Euler_0_10x10_100mgrd_ew.tif
Grid_Mag_Euler_0_10x10_100mgrd_ew.tfw
Grid_Mag_Euler_0_10x10_100mgrd_ns.tif
Grid_Mag_Euler_0_10x10_100mgrd_ns.tfw
Grid_Mag_Euler_0_20x20_10mgrd_ew.tif
Grid_Mag_Euler_0_20x20_10mgrd_ew.tfw
Grid_Mag_Euler_0_20x20_10mgrd_ns.tif
Grid_Mag_Euler_0_20x20_10mgrd_ns.tfw
Grid_Mag_Euler_0_20x20_25mgrd_ew.tif
Grid_Mag_Euler_0_20x20_25mgrd_ew.tfw
Grid_Mag_Euler_0_20x20_25mgrd_ns.tif
Grid_Mag_Euler_0_20x20_25mgrd_ns.tfw
Grid_Mag_Euler_0_20x20_100mgrd_up500_ns.tif
Grid_Mag_Euler_0_20x20_100mgrd_up500_ns.tfw
Grid_Mag_Euler_0_20x20_100mgrd_up500_ew.tif
Grid_Mag_Euler_0_20x20_100mgrd_up500_ew.tfw
Grid_Mag_Euler_0_20x20_100mgrd_up1000_ew.tif
Grid_Mag_Euler_0_20x20_100mgrd_up1000_ew.tfw
Grid_Mag_Euler_0_20x20_100mgrd_up1000_ns.tif
Grid_Mag_Euler_0_20x20_100mgrd_up1000_ns.tfw
Grid_Mag_Euler_1_20x20_10mgrd_ns.tif
Grid_Mag_Euler_1_20x20_10mgrd_ns.tfw
Grid_Mag_Euler_1_20x20_25mgrd_ew.tif
Grid_Mag_Euler_1_20x20_25mgrd_ew.tfw
Grid_Mag_Euler_1_20x20_25mgrd_ns.tfw
Grid_Mag_Euler_1_20x20_25mgrd_ns.tif
Grid_Mag_Euler_2_20x20_25mgrd_ew.tif
Grid_Mag_Euler_2_20x20_25mgrd_ew.tfw
Grid_Mag_Euler_2_20x20_25mgrd_ns.tif
Grid_Mag_Euler_2_20x20_25mgrd_ns.tfw
Grid_Mag_Euler_3_20x20_25mgrd_ew.tif
Grid_Mag_Euler_3_20x20_25mgrd_ew.tfw
Grid_Mag_Euler_3_20x20_25mgrd_ns.tif
Grid_Mag_Euler_3_20x20_25mgrd_ns.tfw
Grid_Mag_Euler_05_3x3_100mgrd_ew.tif
Grid_Mag_Euler_05_3x3_100mgrd_ew.tfw
Grid_Mag_Euler_05_3x3_100mgrd_ns.tif
Grid_Mag_Euler_05_3x3_100mgrd_ns.tfw

7 References

Bastani M, Pedersen L B, 2001. Automatic interpretation of magnetic dike parameters using the analytical signal technique: Geophysics Vol. 66, 551–561.

Bastani M, Pedersen L B, Kero L, 2002. Interpolation of magnetic data enhancing linear features. 64th EAGE conference and exhibition. Extended abstracts Vol. 1, D-33.

Blakely R J, 1995. Potential Theory in Gravity and Magnetic Applications: Canbridge University Press. ISBN 0-521-41508-X.

Isaksson H, Thunehed, H, Keisu M, 2004. Interpretation of airborne geophysics and integration with topography. Stage 1 (2002). SKB P-04-29. Svensk Kärnbränslehantering AB.

Mattsson M, Isaksson H, Thunehed H, 2002. Petrophysical rock sampling, measurements of petrophysical rock parameters and in situ gamma-ray spectrometry measurements on outcrops carried out 2002. SKB P-03-26. Svensk Kärnbränslehantering AB.

Reid A B, Allsop J M, Granser H, Millet A J, Somerton I W, 1990. Magnetic interpretation in three dimensions using Euler Deconvolution. Geophysics Vol. 55. pp 80–91.

Rönning H J S, Kihle O, Mogaard J O, Walker P, Shomali H, Hagthorpe P, Byström S, Lindberg H, Thunehed H, 2003. Forsmark site investigation. Helicopter borne geophysics at Forsmark, Östhammar Sweden. SKB P-03-41. Svensk Kärnbränslehantering AB.

Stephens M B, Bergman T, Andersson J, Hermansson T, Wahlgren C-H, Albrecht L, Mikko H, 2003. Forsmark Bedrock mapping. Stage 1 (2002) - Outcrop data including fracture data. SKB P-03-09. Svensk Kärnbränslehantering AB.

Thompson D T, 1982. EULDPH: A new technique for making computer-assisted depth estimates from magnetic data. Geophysics Vol. 47. pp 31-37.